GABAergic inhibition shapes interictal dynamics in awake epileptic mice

Sarah Feldt Muldoon, Vincent Villette, Thomas Tressard, Arnaud Malvache, Susanne Reichinnek, Fabrice Bartolomei, Rosa Cossart

GABAergic inhibition shapes interictal dynamics in awake epileptic mice

Sarah Feldt Muldoon,[1,2,3,*,†] Vincent Villette,[1,2,3,*] Thomas Tressard,[1,2,3] Arnaud Malvache,[1,2,3] Susanne Reichinnek,[1,2,3] Fabrice Bartolomei[4] and Rosa Cossart[1,2,3]

*These authors contributed equally to this work.

Epilepsy is characterized by recurrent seizures and brief, synchronous bursts called interictal spikes that are present in-between seizures and observed as transient events in EEG signals. While GABAergic transmission is known to play an important role in shaping healthy brain activity, the role of inhibition in these pathological epileptic dynamics remains unclear. Examining the microcircuits that participate in interictal spikes is thus an important first step towards addressing this issue, as the function of these transient synchronizations in either promoting or prohibiting seizures is currently under debate. To identify the microcircuits recruited in spontaneous interictal spikes in the absence of any proconvulsive drug or anaesthetic agent, we combine a chronic model of epilepsy with *in vivo* two-photon calcium imaging and multiunit extracellular recordings to map cellular recruitment within large populations of CA1 neurons in mice free to run on a self-paced treadmill. We show that GABAergic neurons, as opposed to their glutamatergic counterparts, are preferentially recruited during spontaneous interictal activity in the CA1 region of the epileptic mouse hippocampus. Although the specific cellular dynamics of interictal spikes are found to be highly variable, they are consistently associated with the activation of GABAergic neurons, resulting in a perisomatic inhibitory restraint that reduces neuronal spiking in the principal cell layer. Given the role of GABAergic neurons in shaping brain activity during normal cognitive function, their aberrant unbalanced recruitment during these transient events could have important downstream effects with clinical implications.

1 Institut National de la Santé et de la Recherche Médicale Unité 901, 13009 Marseille, France
2 Aix-Marseille Université, Unité Mixte de Recherche S901, 13009 Marseille, France
3 Institut de Neurobiologie de la Méditerranée, 13009 Marseille, France
4 Institut des Neurosciences des Systèmes, Institut National de la Santé et de la Recherche Médicale Unité 1106, 13005 Marseille, France

†Present address: Department of Mathematics and Computational Data Science and Engineering Program, University at Buffalo, SUNY, Buffalo, NY 14260, USA

Correspondence to: Dr Rosa Cossart,
Institut de Neurobiologie de la Méditerranée,
INMED UMR901,
Parc Scientifique de Luminy BP 13,
13273 Marseille cedex 09,
France
E-mail: rosa.cossart@inserm.fr

Keywords: epilepsy; interictal spikes; calcium imaging; GABA; microcircuits

Abbreviations: kCSD = kernel current source density; TLE = temporal lobe epilepsy

Introduction

Interictal spikes are an electrophysiological marker of epilepsy (Gibbs *et al*., 1935) that occur much more frequently than seizures. These transient EEG signals are characterized by a short duration (<100 ms), large amplitude, and can be classified as multiphasic or single spikes (Huneau *et al*., 2013), which usually include a sharp spike followed by a slower wave. For clinical reasons, less significance is given to interictal spikes than to ictal events, as the former are not associated with any salient clinical manifestation. However, even in seizure-free patients, interictal spikes may lead to transitory cognitive impairment (Binnie, 2003) and episodic interictal memory disturbances (Mosbah *et al*., 2014). Furthermore, the function of these spikes is highly debated and has been proposed both as a protective phenomenon against the emergence of paroxysmal activities (de Curtis and Avanzini, 2001), or conversely, as a prelude to seizures (Staley *et al*., 2011). Similar to seizures, interictal spikes can originate from multiple foci and propagate to the surrounding regions through multiple paths (Chagnac-Amitai and Connors, 1989; Badier and Chauvel, 1995). In fact, in temporal lobe epilepsy (TLE), interictal spiking frequently originates from multiple subsets of temporal lobe structures, sometimes outside of the epileptogenic zone (Bourien *et al*., 2005).

The study of interictal spikes is therefore of special interest because, despite their association with epileptogenesis (Staley *et al*., 2011; Avoli *et al*., 2013; Huneau *et al*., 2013), their diagnostic yield (Blume *et al*., 2001), possible causal link to seizures (Avoli *et al*., 2013), and relationship to cognitive impairment, little is known about the specific microcircuits recruited throughout their propagation. Given the dual role of GABAergic circuits in dampening excitation and in coordinating the network oscillations that support cognitive function, it is therefore critical to specifically examine the spatio-temporal patterns of micro-scale inhibitory function.

One of the early identified possible roles of inhibition in epileptiform discharges was that of a restraint, or an 'inhibitory surround' that would function to oppose the spread of epileptic activity, thus creating an area of uncorrelated and sparsely propagating activity around the epileptogenic zone (Prince and Wilder, 1967). This phenomenon has been particularly well documented in human patients or drug-induced models of neocortical epilepsy in relation to ictal events (Prince and Wilder, 1967; Dichter and Spencer, 1969*a*, *b*; Trevelyan *et al*., 2006; Trevelyan, 2009; Sabolek *et al*., 2012; Schevon *et al*., 2012; Trevelyan and Schevon, 2013). Alternatively, it has been proposed that GABAergic transmission could initiate the synchronization process leading to paroxysmal discharges in the hippocampal formation of patients with drug-resistant TLE (Alvarado-Rojas *et al*., 2013). Although this debate has yet to be resolved, it is clear that the relation between interictal spiking and single-cell activity depends both on the type of epilepsy and the recording site, and is more heterogeneous than simple paroxysmal depolarization shifts (Prince and Wilder, 1967; Dichter and Spencer, 1969*a*, *b*; Trevelyan *et al*., 2006; Zhou *et al*., 2007; Trevelyan, 2009; Keller *et al*., 2010; Truccolo *et al*., 2011; Sabolek *et al*., 2012; Schevon *et al*., 2012; Alvarado-Rojas *et al*., 2013; Feldt Muldoon *et al*., 2013; Trevelyan and Schevon, 2013).

In TLE, the hippocampus is often linked to the site of seizure initiation, and here, epileptogenesis has been traditionally associated with GABAergic cell death and an overall dysfunction of inhibition. However, it is becoming increasingly clear that the diversity of GABAergic cell fates during epileptogenesis mirrors the morpho-functional heterogeneity of this cell population (Cossart *et al*., 2005). While some GABAergic microcircuits are selectively destroyed during epileptogenesis, those that are spared can be functionally (Chen *et al*., 2001; Cossart *et al*., 2001; Marchionni and Maccaferri, 2009) and/or anatomically (Nusser *et al*., 1997; Peng *et al*., 2013) boosted.

To fully understand the contribution of this modified inhibitory circuitry in shaping interictal dynamics, it is additionally important to study epileptic activity in the absence of anaesthetics. Recently, it has become clear that anaesthetics can modify neuronal activity, and firing rates and spike bursting have been shown to be higher, and correlated activity weaker, in awake compared to anaesthetized rats (Greenberg *et al*., 2008). Therefore, one must quantify the exact contribution of spatially distributed distinctive neurons to epileptiform dynamics under awake, *in vivo* conditions to fully understand how these diverse microcircuits contribute to pathological activity.

To this aim, we used a chronic model of TLE and studied spontaneous neuronal dynamics in the CA1 region of awake head restrained mice, free to run on a self-paced treadmill, using combined electrophysiological and two-photon calcium microscopy techniques. Although TLE mice displayed both interictal as well as ictal activity, we restricted our study to spontaneous interictal spikes, as the probability of observing a seizure was extremely low (see the Supplementary material for a discussion of seizure dynamics). Here, we focus our efforts on studying the spatial patterns of cellular recruitment during interictal spikes that propagate through the CA1 region of the hippocampus. CA1 is a very commonly studied region in the framework of epilepsy (Cossart *et al*., 2001; Bernard *et al*., 2004; Krook-Magnuson *et al*., 2013) and, through a dysregulated temporoammonic pathway, serves as an entry point into the hippocampus that enables the propagation of epileptiform activity directly from the entorhinal cortex, bypassing the classical trisynaptic loop (Wozny *et al*., 2005; Ang *et al*., 2006).

To isolate the recruitment of GABAergic microcircuits during interictal spikes, we additionally used a transgenic mouse line that allows for the restricted viral expression of a calcium reporter protein in only these cells (Tolu *et al*., 2010; Melzer *et al*., 2012). We found that during interictal

spikes, CA1 inhibition is synchronized, which leads to the quieting of neurons in the pyramidal cell layer. Therefore, we identify a dysfunction of the CA1 feedforward inhibitory microcircuit that potentially acts as an inhibitory brake to the propagation of epileptiform dynamics from the hippocampus to the rest of the brain (Prince and Wilder, 1967; Dichter and Spencer, 1969*a*, *b*; Trevelyan *et al.*, 2006; Trevelyan, 2009; Sabolek *et al.*, 2012; Schevon *et al.*, 2012; Trevelyan and Schevon, 2013), and contributes to a functional deafferentation of the subiculum (Cohen *et al.*, 2002; Wozny *et al.*, 2003), even in the absence of hippocampal sclerosis. This finding challenges the intuitive view that epilepsy results from an imbalance of inhibitory and excitatory action in favour of runaway excitation and instead supports earlier work (Prince, 1968; Velazquez and Carlen, 1999; Cohen *et al.*, 2002; Klaassen *et al.*, 2006; Zhou *et al.*, 2007; Marchionni and Maccaferri, 2009; Avoli and de Curtis, 2011; Huberfeld *et al.*, 2011) as well as theoretical predictions (Li *et al.*, 2008) indicating that the GABAergic microcircuits that are spared in the course of epileptogenesis contribute in shaping interictal discharges.

Materials and methods

Here we present a condensed version of the experimental and analytical methods. For complete descriptions, please see the Supplementary material. All protocols were performed under the guidelines of the French National Ethic Committee for Sciences and Health report on 'Ethical Principles for Animal Experimentation' in agreement with the European Community Directive 86/609/EEC under agreement #01413.03. Unless otherwise noted, all analysis was carried out in MATLAB using custom-made code, which can be provided by the authors upon request. Error bars denote standard error of the mean (SEM), and when necessary, Kolmogorov-Smirnov tests were used to assess the normality of distributions. Sample sizes were chosen to ensure experimental reproducibility and robustness while minimizing animal distress.

The pilocarpine model of temporal lobe epilepsy

Male adult wild-type Swiss mice ($n = 14$) or GAD67-Cre mice (Tolu *et al.*, 2010; Melzer *et al.*, 2012) ($n = 4$) crossed onto a Swiss background were used for experiments. As previously described (Feldt Muldoon *et al.*, 2013), mice were subjected to the pilocarpine model of TLE (Cavalheiro *et al.*, 1996). To ensure that the mice had reached the chronic phase of the model (displayed both interictal spikes and seizures), we waited an average of 58 ± 11 days (range 26–136) between pilocarpine injections and the first recording session (Supplementary Fig. 1A).

Interictal spike detection

To detect the occurrence of spontaneous interictal spikes, mice were implanted contralaterally with a global cortico-hippocampal electroencephalogram (contralateral EEG), hippocampal local field potential (contralateral LFP) and neck electromyogram (EMG) as shown in Fig. 1A. Interictal spikes were semi-automatically detected from the electrophysiological data simultaneously recorded in the contralateral hemisphere during imaging/probe recording sessions using custom-made software written in MATLAB. First, to remove noise artefacts, contralateral EEG and contralateral local field potential signals were filtered between 1 and 25 Hz using a fourth order Butterworth filter, and a threshold value was calculated using a moving standard deviation of the filtered signal over a 5-s sliding window (Supplementary Fig. 1B). Potential spikes were selected as points where both the filtered contralateral EEG and contralateral local field potential signals exceed this threshold. Potential spikes were then visually compared to the EMG signal to separate true spikes from movement artefacts, and the start and end times of the spike were manually marked using the unfiltered signal.

Linear probe recordings

A 16-channel linear silicon probe was used to obtain acute recordings of the LFP depth profile of the CA1 region in TLE mice ($n = 4$ mice). The spatial properties describing sinks and sources during interictal spikes were evaluated using the 13 channel LFPs from these linear probe recordings and a kernel current source density method (kCSD, for further details see Potworowski *et al.*, 2012). In one mouse of the four used for the probe experiments, the recorded signal saturated the amplifier during the spikes so this mouse was discarded from the kCSD analysis. Additionally, in one other mouse, obvious movement artefacts occurred during seven interictal spikes so these spikes were also removed from the analysis. This resulted in a final analysis of $n = 158$ interictal spikes recorded from three mice. To analyse the multiunit activity of pyramidal cells, the probe channel in which unit activity could be seen visually was selected for multiunit detection. The signal was first zero phase digitally filtered between 300 and 3000 Hz using a fourth order Butterworth filter. A baseline movement-free period of 10 s was selected, and multiunit activity was detected as points in time where the signal exceeded a threshold of five times the standard deviation of the baseline signal. To compare firing rates before and after interictal spikes, the average firing rate was calculated for a 500-ms window immediately before and immediately after each spike. In one of the four mice used, we could not detect unit activity in any of the recorded channels and thus this mouse was discarded from further analysis, meaning that the analysis was performed over $n = 131$ interictal spikes recorded from three mice.

Calcium imaging

To perform large-scale calcium imaging, wild-type TLE mice were injected with a viral solution of either GCaMP5G ($n = 3$), GCaMP6m ($n = 3$), or TLE GAD67-Cre mice with a viral vector carrying a CRE-dependent version of GCaMP5G. This procedure induced the expression of the GCaMP indicator in all neurons within the field of view, as quantified using immunohistochemical analysis (Supplementary Fig. 2). To allow optical access to the hippocampus, a ~3-mm diameter craniotomy centred over injection sites was performed: the

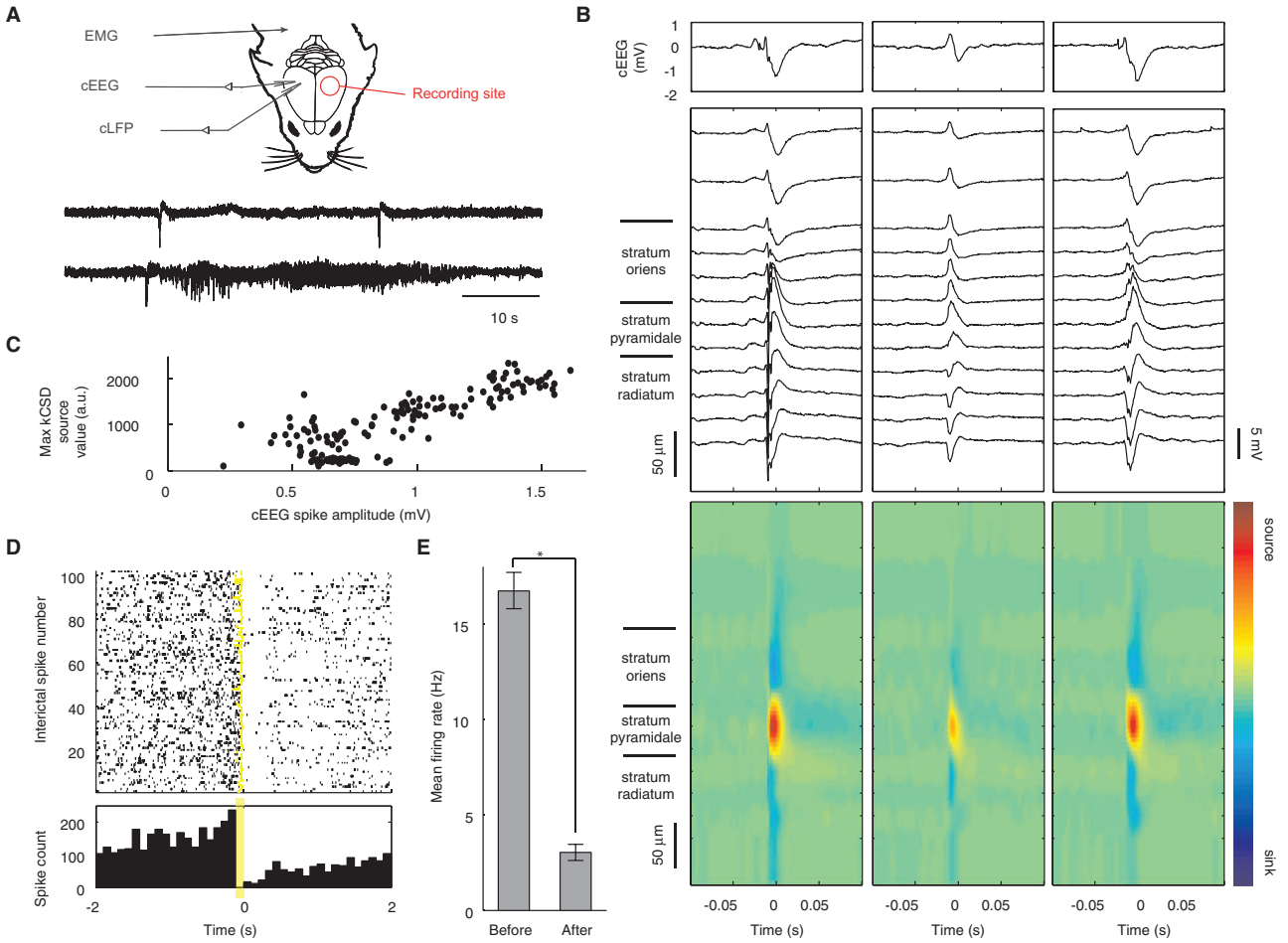

Figure 1 Electrophysiological properties of interictal spikes in CA1. (**A**) Schematic of chronic contralateral electrode placement and ipsilateral recording site (*upper*), contralateral EEG traces showing interictal spikes (*middle*) and ictal activity (lower). (**B**) Contralateral EEG (cEEG, *top*), linear probe recordings (*middle*), and corresponding kCSD analysis (*bottom*) for three interictal spikes from the same mouse. (**C**) Correlation between contralateral EEG and kCSD source amplitudes (Spearman's $\rho = 0.79$, $P < 0.001$, $n = 158$ interictal spikes from three mice). (**D**) Raster plot (*top*) and corresponding histogram (*bottom*) of multiunit activity in the stratum pyramidale for $n = 102$ interictal spikes from one mouse where $t = 0$ indicates spike time. Yellow boxes indicate time excluded due to the spike artefact. (**E**) Mean multiunit firing rate of stratum pyramidale cells 500 ms immediately before and after the spike (two-sample *t*-test, $P < 0.001$, $n = 131$ interictal spikes from three mice). Error bars represent SEM.

dura was gently cut and a small portion of the cortex was aspirated. A chronic glass window was implanted as previously reported (Dombeck *et al.*, 2010) but adapted slightly for large-scale imaging (Supplementary Fig. 1C). Although this procedure did involve the removal of a small portion of the cortex, the cortex was not removed for the linear probe recordings, and the spikes recorded on the contralateral EEG showed the same variability under both conditions. Additionally, all results are consistent between linear probe experiments and imaging experiments, so we conclude that our observations are not likely to be significantly affected by the surgical procedure.

All mice were handled before recording sessions to limit head restraint associated stress.

During imaging, mice were head-fixed on a non-motorized treadmill (adapted from Royer *et al.*, 2012) that allowed for self-paced locomotion to limit stress (Supplementary Fig. 1D). All experiments were performed in the dark. No rewards were given and the mice alternated between periods of moving and resting activity during recordings. The fluorescence activity from a 400 × 400 µm field of view (500 × 500 µm for × 20 objective) was acquired at ~7.7 Hz and recordings lasted ~4.5 min. Mice were imaged over multiple days (range 2–16 days). During imaging sessions, mice displayed spontaneous interictal spikes as detected in the contralateral EEG signal and these spike times were aligned with the corresponding movie frames through *post hoc* analysis.

For calibration experiments, mice ($n = 28$) were anaesthetized with ketamine (100 mg/kg) and xylazine (10 mg/kg) for surgery. A reference electrode was placed above the contralateral cerebellum and a glass coverslip with a hole allowing for pipette insertion covered hippocampal fibres. During recordings, a supplemental anaesthetic was provided if necessary (urethane, 1.5 g/kg, Sigma). Juxtacellular recordings were acquired using glass pipettes with a MultiClamp 700B Amplifier (Axon Instrument) and digitized at 20 kHz (Digidata1440a, Axon Instrument) while imaging as described above.

Spatial imprint analysis

To analyse the spatial patterning of cells recruited during interictal spikes, we calculated the 'spatial imprint' for each spike. Spatial imprints are composed of the pixel-by-pixel percentage change in fluorescence during a given interictal spike and therefore serve as a visual representation of the pixels activated during the spike. An image of baseline activity was created by averaging the movie frames acquired during a 500 ms window immediately preceding (but not including) the interictal spike (Supplementary Fig. 1E: 'Before image'). Similarly, an image representing the activity recorded during the spike was created by averaging the movie frames acquired during a 500-ms window immediately after (and including) the interictal spike (Supplementary Fig. 1E: 'After image'). We then produced the spatial imprint for each event by computing the dF/F image for the event, i.e. for each pixel, we calculated the change in fluorescence as (Image_after − Image_before) / Image_before. The spatial imprint is thus a normalized image that represents the spatial patterning of cell bodies and processes activated during each interictal spike, i.e. pixels that were active (experienced an increase in fluorescence) during the event appear brighter than those that were not active. In Supplementary Fig. 1E, the red arrow indicates a cell that did not participate in the spike, while the green arrow indicates a cell that was recruited during the spike.

Results

To identify the microcircuits recruited in spontaneous interictal spikes in the absence of any proconvulsive drug or anaesthetic agent, for the first time, we recorded electrical and optical signals from chronically epileptic awake mice using the pilocarpine model of TLE (Cavalheiro *et al.*, 1996). This widely used chronic model of epilepsy (Brooks-Kayal *et al.*, 1998; Cossart *et al.*, 2001; Smolders *et al.*, 2002; Fabene *et al.*, 2008; Hunt *et al.*, 2013) was chosen not only because spontaneous recurrent interictal spikes and seizures occur following an initial brain insult, but also because the development of such epileptiform activity has been associated with several well-described behavioural and structural network changes that reproduce the human pathology. Recordings from awake mice were achieved using head-restrained animals, allowed to self-regulate their motion on a non-motorized treadmill (Royer *et al.*, 2012). During each recording session, mice spontaneously alternated between run and rest periods, as their behaviour was not guided toward any reward.

Interictal spikes suppress multiunit activity in pyramidal cell layer

To observe epileptiform activities, TLE mice were chronically implanted with a contralateral macroscopic surface electroencephalogram (contralateral EEG), hippocampal CA1 local field potential (contralateral local field potential), and neck electromyogram (EMG) (Fig. 1A). Mice displayed spontaneous interictal spikes and seizures as observed in the contralateral EEG signal (Fig. 1A). Neuronal activity was then monitored ipsilaterally in the CA1 region of the hippocampus using either acute electrophysiological recordings with a linear silicone probe ($n = 171$ interictal spikes from four mice) or chronic two-photon calcium imaging ($n = 2619$ interictal spikes from 10 mice). The contralateral EEG signal was used for interictal spike detection, as these occurred simultaneously with local ipsilateral CA1 interictal spikes observed in linear probe recordings spanning the deeper neocortical layers down to the stratum radiatum (Supplementary Fig. 3). As previously described, interictal spikes are polymorphic events (Buzsaki *et al.*, 1991; Chauviere *et al.*, 2012) and all probe channels therefore expressed a wide heterogeneity in the interictal spike shape from event to event. However, kCSD analysis consistently revealed a source in the CA1 pyramidal cell layer (Fig. 1B). Interestingly, the strength of this local source was highly correlated with the amplitude of the global contralateral EEG spike (Fig. 1C, Spearman's $\rho = 0.79$, $n = 158$ interictal spikes from three mice). Although a source in the CA1 pyramidal layer is often produced by synchronous neuronal firing, it could also originate from a phasic perisomatic inhibitory input, and further information is needed to address this ambiguity (Buzsaki *et al.*, 2012). We therefore first examined multiunit activity in the CA1 pyramidal cell layer within a 2-s window centred on each interictal spike. Analysis revealed that multiunit frequency decreased immediately following interictal spikes, and this was consistently observed across all events in all animals (Fig. 1D and E, firing rate 500 ms before interictal spike = 16.7 ± 0.9 Hz, firing rate 500 ms after interictal spike = 3.0 ± 0.4 Hz, $n = 131$ interictal spikes from three mice). This striking result indicates that the kCSD source was likely due to pyramidal cells receiving a strong inhibition. Unfortunately, multiunit activity of pyramidal cells could not be assessed directly during the interictal spike due to the spike artefact (indicated by the yellow boxes in Fig. 1D), and we therefore turned to calcium imaging to further investigate cellular activity during the interictal spikes.

Calcium imaging of spontaneous interictal spikes

We used a viral vector to express the calcium reporter protein GCaMP5G ($n = 3$ mice) or GCaMP6m ($n = 3$ mice) in CA1 hippocampal cells (Akerboom *et al.*, 2012; Chen *et al.*, 2013). We adapted the surgical implantation of a previously described chronic window on the hippocampus that was shown to allow for the visualization of place cell firing (Dombeck *et al.*, 2010). This procedure allows for direct imaging of spontaneous activity in the stratum oriens (a layer with mostly somata of GABAergic neurons) and stratum pyramidale (mainly somata of glutamatergic principal cells) during interictal spikes over several days (range 2–16 days). All reported results were robust

throughout the entire imaging period. As with probe experiments, the detection of interictal spikes was based upon the contralateral EEG signal. During periods free of interictal spikes, cells were spontaneously active with more activity in the stratum pyramidale observed during periods of running, consistent with calcium imaging of non-epileptic, wild-type mice (Supplementary Fig. 4 and Supplementary Video 1).

In vivo two-photon imaging using GCaMP reporters has been previously used in the hippocampus to report bursting dynamics in place cells (Dombeck *et al.*, 2010) or to map neuronal activation during fear learning (Lovett-Barron *et al.*, 2014). However, it is important to understand if these reporters can reliably capture single-cell activation under conditions with lower neuronal firing rates. Although the GCaMP reporters have been shown to be sensitive to single action potential firing in the upper layers of the visual cortex *in vivo* (Chen *et al.*, 2013), it is unclear if these results hold under our conditions. As simultaneous imaging and patch-clamp recording is difficult under the hippocampal window, in order to probe the reliability of our experimental procedure for single action potential detection, we first tested whether we could detect the calcium transients associated with ripple events, a well-described physiological activity pattern that is known to produce single-spikes in CA1 pyramidal neurons within a similar time window as the interictal spikes (Csicsvari *et al.*, 1999; Gulyas and Freund, 2014). We detected ripple events in the contralateral local field potential of wild-type, non-epileptic mice ($n = 2$ mice) and observed time-locked calcium transients in stratum pyramidale neurons. These transients were of smaller amplitude than those associated with place-modulated firing, further indicating that they were produced by a few, if not single, spikes (Supplementary Fig. 5). In addition, using juxtacellular recordings from anaesthetized mice, we were able to record calcium signals in stratum pyramidale that aligned with the firing of action potentials and confirmed that sparse firing (approximately two to three spikes) produced significant calcium transients in these cells ($n = 4$ cells, Supplementary Fig. 6). Altogether, this indicates that our imaging set-up allows for the detection of single-cell activation during synchronous events, even when single-cell firing rate is low. Although the time resolution of the imaging does not allow for the evaluation of temporal sequences of cellular activation during these fast events, it instead provides information concerning the spatial patterning of cells that participate (or not) in events.

In both the stratum oriens and the stratum pyramidale, interictal spikes appeared as global flashes in the calcium movies (Fig. 2A and Supplementary Videos 2 and 3), indicating a large calcium rise throughout the CA1 region ($n = 1396$ interictal spikes from six mice). To examine the spatial patterning of cells involved in these spikes, we created a 'spatial imprint' of each interictal spike, i.e. an image that allows for the visualization of cell bodies and processes that were active during the event (Fig. 2B and C). In the spatial imprints of interictal spikes, we consistently observed a diffuse spatial patterning in the stratum pyramidale (Fig. 2B), compared to the clearly visible activation of somata and processes in the stratum oriens (Fig. 2C). Yet, when we pool all events (distributed throughout all observable imaging depths across both the stratum oriens and stratum pyramidale), we see a supralinear correlation between the amplitude of the spike recorded by the contralateral EEG and the amplitude of the fluorescence change associated with the interictal spike (Fig. 2D), with no dependence upon the depth of imaging. Thus the diffuse activation pattern observed in the stratum pyramidale followed the same relation as the spatially defined cellular activation patterns in the stratum oriens.

Differential recruitment of cells in stratum oriens versus pyramidale

To investigate further the relationship between firing of individual cells and the global calcium transient, we studied the dynamics of individual cells in both the stratum oriens and stratum pyramidale during interictal spikes using both the GCaMP5G and the more sensitive GCaMP6m variants of the reporter. Although one can see a faint increase in an individual cell's GCaMP signal during the interictal spike (Fig. 3A and B), cells show larger increase outside of events, indicating that cells with a soma in the stratum pyramidale are firing more when active outside of the interictal spike than during the spike. The same phenomenon was observed regardless of the indicator used (5G/6 m) so data from the two indicators were pooled for the remaining analysis.

To detect differences in neuronal recruitment during an interictal spike when imaging in the stratum oriens versus stratum pyramidale, we next compared the percentage of cells displaying a significant increase in the calcium signal (i.e. recruited cells) during large interictal spikes (i.e. interictal spikes with an average dF/F amplitude $>50\%$). Due to the differences in the density of cells between the stratum pyramidale and stratum oriens (Fig. 3D), we quantified the percentage of imaged cells that were recruited during interictal spikes, but absolute numbers of cells are also reported (Table 1). The percentage of neuronal recruitment in the stratum pyramidale was remarkably low (Fig. 3C, median = 0.6%), which represented a significantly lower fraction of cells than observed in the stratum oriens (Fig. 3C, median = 33%, two-sample Kolmogorov-Smirnov test, $P > 0.001$). This low percentage of active cells in the stratum pyramidale corresponds to, on average, 4 ± 1 cells (out of an estimated 766 ± 47 imaged cells in the stratum pyramidale) that are recruited during interictal spikes. On the contrary, in the stratum oriens, we see that a much higher fraction of cells are recruited (on average 2.1 ± 0.3 of a total of 7 ± 1 imaged cells), although this distribution is widespread and highly variable from event to event.

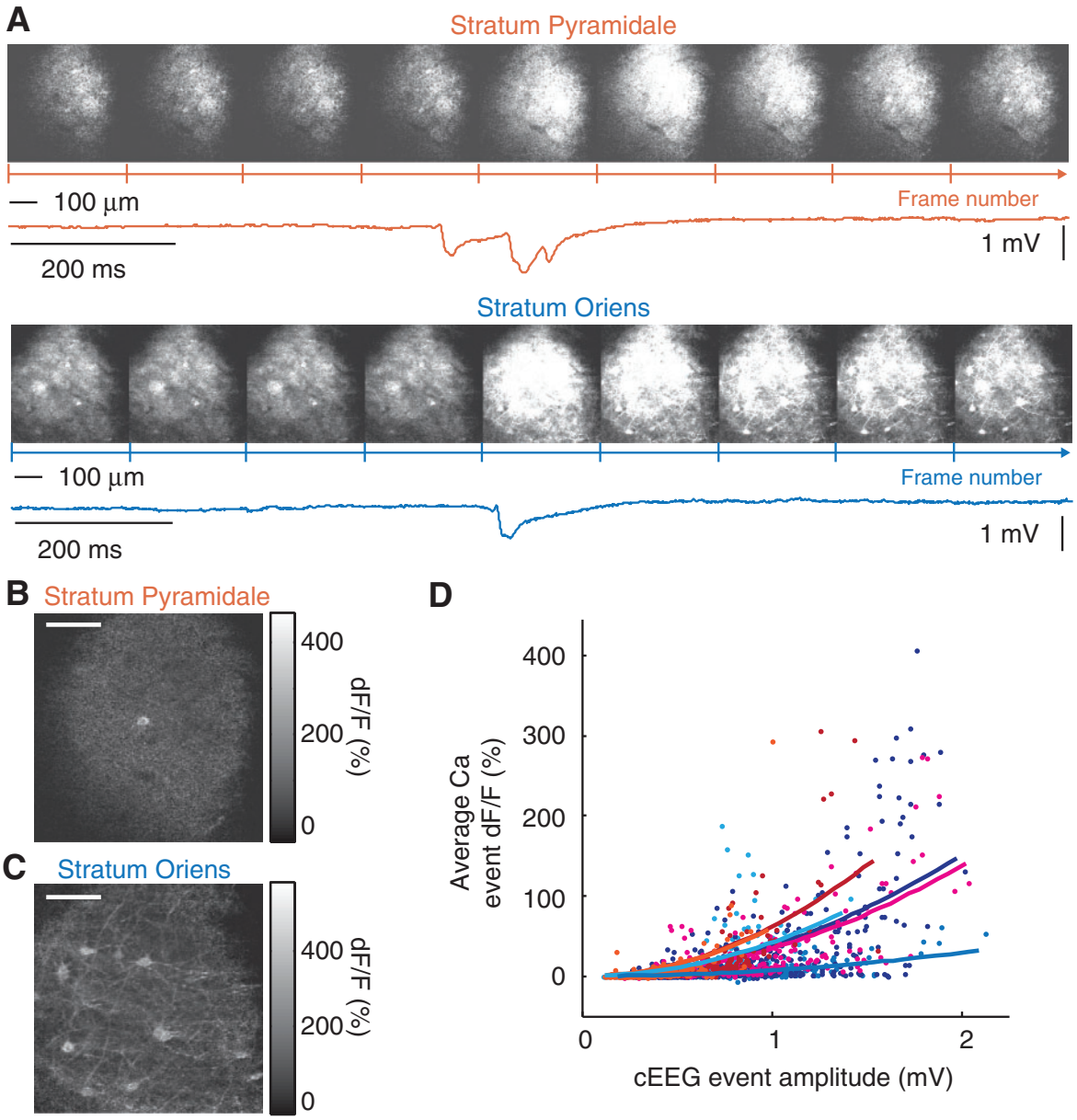

Figure 2 Calcium imaging of CA1. (**A**) Successive movie frames and simultaneous contralateral EEG signal for an interictal spike imaged in the stratum pyramidale (orange, Supplementary Video 2) or in the straum oriens (blue, Supplementary Video 3). (**B** and **C**) Corresponding spatial imprint during an interictal spike imaged in the stratum pyramidale (**B**) and stratum oriens (**C**). Scale bar represents 100 µm. (**D**) Relationship between the amplitude of the contralateral EEG and the average image dF/F during interictal spikes. Blue shades: GCaMP5 (n = 3 mice, 855 interictal spikes), red shades: GCaMP6 (n = 3 mice, 541 interictal spikes). Data from the stratum pyramidale and stratum oriens are pooled since the relationship was independent of the imaging location.

To further examine the sparse activation of cells in the stratum pyramidale, we additionally computed the number and percentage of cells that were active outside of interictal spikes (Table 1 and the Supplementary material). More pyramidal cells were active outside of interictal spikes (38 ± 10 cells) than during spikes (3.7 ± 0.7 cells). Even if the percentage of cells in the stratum pyramidale recruited during interictal spikes is calculated out of the number of cells that are active at some point outside of the spikes, the percentage of cells recruited during spikes rises only to an average value of $19.5 \pm 3.8\%$. Interestingly, as seen in the individual examples of cellular recruitment during interictal spikes, depicted in Fig. 3E, in the stratum pyramidale and stratum oriens, different subsets of cells are recruited in sequential events. Taken together, these results indicate that, while only subpopulations of cells participate in interictal spikes in both the stratum oriens and stratum pyramidale, the GABAergic cells located in the stratum oriens are more likely to be recruited during events. Given the lack of

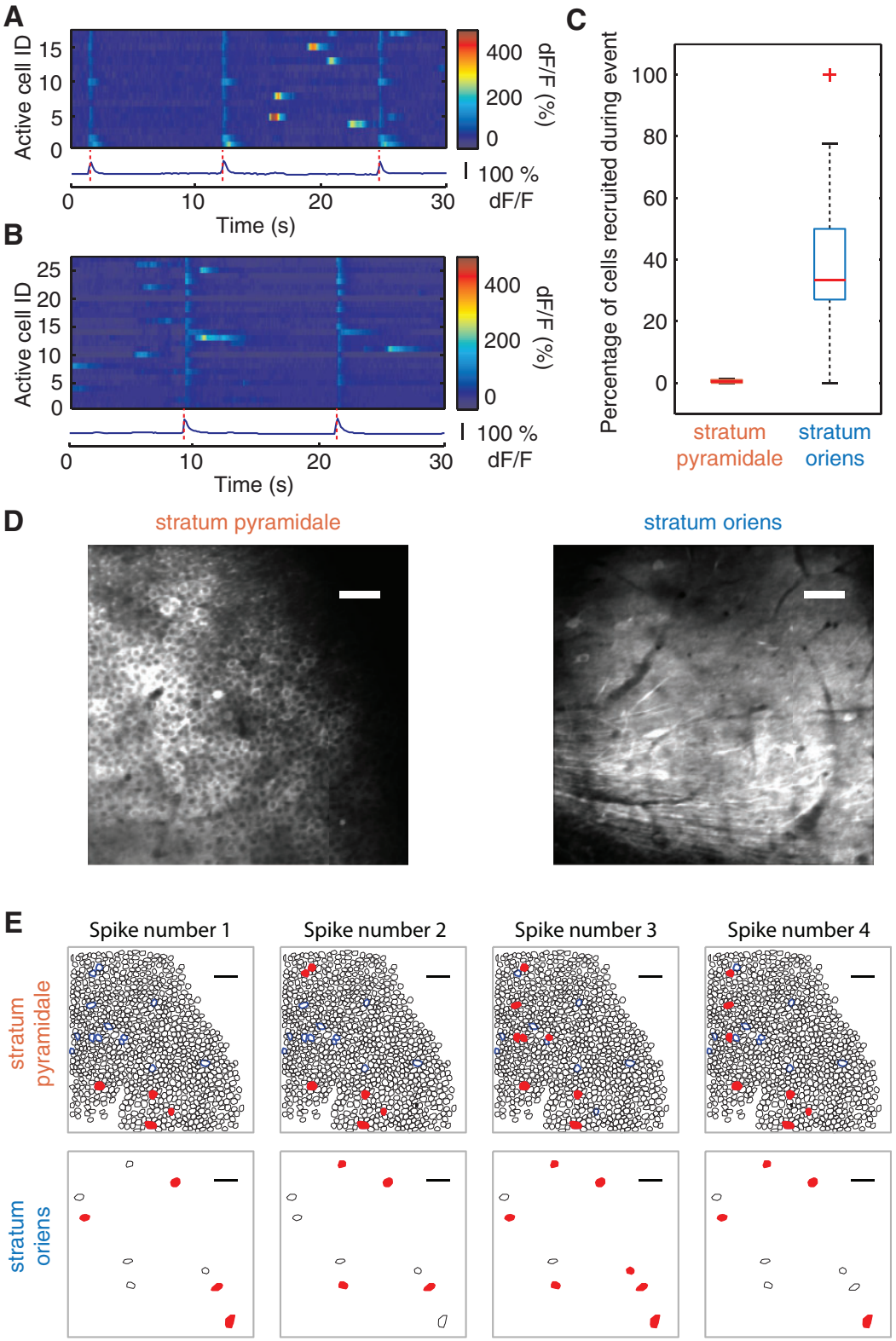

Figure 3 Single-cell participation in interictal spikes. (**A**) GCaMP5 signal from active cells (*top*) and corresponding dF/F averaged over the entire imaging area. Dashed red lines indicate the occurrence of interictal spikes. (**B**) Same as (**D**) for GCaMP6. (**C**) Distribution of the percentage of detected cells that were active during interictal spikes (stratum pyramidale median = 0.6 %, n = 29 interictal spikes from six mice; stratum oriens median = 33.3%, n = 33 interictal spikes from six mice; statistically different: two-sample Kolmogorov-Smirnov test, $P << 0.001$). (**D**) Images of the average GCaMP signal in the stratum pyramidale (*left*) and stratum oriens (*right*) corresponding to the contours of cells depicted in (**E**). Scale bars = 50 μm. (**E**) Contours of imaged cells in a single movie from the stratum pyramidale (upper, n = 827 cells) and stratum oriens (lower, n = 9 cells). Blue contours in the stratum pyramidale indicate cells that were active outside of interictal spikes. Red filled contours indicate cells recruited during a single interictal spike, and data are shown for four consecutive interictal spikes. Scale bars = 50 μm.

Table 1 Cellular recruitment during interictal spikes

	Stratum pyramidale	Stratum oriens
Number of imaged cells	766 ± 47	7 ± 1
Number of cells recruited in interictal spikes	3.7 ± 0.7	2.1 ± 0.3
Percentage of imaged cells recruited in interictal spikes	0.5 ± 0.1%	38.6 ± 4.0%
Number of active cells (outside interictal spikes)	38 ± 10	
Percentage of active cells (outside interictal spikes)	4.7 ± 1.1%	
Percentage of active cells recruited in interictal spikes	19.5 ± 3.8%	

cellular participation of cells in the stratum pyramidale combined with the supralinear relationship between the contralateral EEG amplitude and calcium response, which was independent of imaging location, this leaves GABAergic perisomatic innervation as a likely candidate for the observed diffuse increase in GCaMP fluorescence in the stratum pyramidale.

GABAergic neurons are the main participants in interictal spikes in CA1

To further test whether GABAergic cells are the main contributors to the GCaMP fluorescence signal associated with interictal spikes, we next performed imaging in TLE GAD67-Cre mice injected with a viral vector carrying a CRE dependent version of GCaMP5G (Tolu *et al.*, 2010). Here, the calcium reporter is only expressed in GABAergic cells, and the associated fluorescence signal originates solely from GABAergic neurons. GCaMP5G could be detected in the soma and dendrites, as well as in putative perisomatic axonal terminals located in the stratum pyramidale (Fig. 4A). As observed in wild-type TLE mice, interictal spikes in both the stratum pyramidale and stratum oriens were associated with transient increases in the GCaMP signal (Fig. 4B, Supplementary Videos 4 and 5, $n = 1223$ spikes from four mice). The spatial imprint of interictal spikes imaged in the stratum pyramidale clearly indicated the activation of GABAergic processes throughout the pyramidal layer (Fig. 4C), and events in the stratum oriens were confirmed to originate from the activation of a subset of cell bodies from GABAergic neurons and a web of putative dendritic processes (Fig. 4D). Importantly, we also observed the same supralinear correlation between the amplitude of the recorded contralateral EEG spike and the amplitude of the corresponding change in GCaMP fluorescence under these conditions where only GABAergic cells contributed to the GCaMP signal (Fig. 4C, Functional Data Analysis, non-parametric permutation test, no difference between groups, $P = 0.54$). Thus, the observed calcium response is the same with or without the inclusion of signals from the glutamatergic population, confirming that in CA1, the fluorescence increase during interictal spikes is driven by the activation of GABAergic cells.

Spatial patterning of local recruitment varies between interictal spikes and follows macro-scale variable dynamics

Given that GABAergic inhibition was previously identified as a possible circuit mechanism for the variable paths by which synchronous activity spreads through epileptic networks (Sabolek *et al.*, 2012), we asked whether a related variability in the recruitment of GABAergic microcircuits could be observed *in vivo*. We therefore developed an analysis to compare the spatial similarity of interictal spikes imaged in GAD67-Cre mice (Fig. 5). A similarity matrix of the spatial overlap between interictal spikes was run through a hierarchical clustering algorithm to group events with similar spatial patterning (Fig. 5A–D and Supplementary material). Matrices were resorted with respect to the results of the clustering algorithm and visually inspected for the appearance of communities (i.e. groups of neurons with similar firing patterns within the group but different from those outside the group, and visible as block-like structures along the diagonal of the sorted similarity matrix). Clear community structure was visible in the similarity matrix in five of eight analysed imaging sessions (coloured boxes in Fig. 5D), indicating that interictal spikes within a community had the same spatial structure, but that this structure was different for interictal spikes between communities, and that sequential spikes do not necessarily recruit the same population of GABAergic neurons (Fig. 5C). Therefore, we conclude that variable subpopulations of GABAergic cells compose the specific microcircuitry activated during interictal spikes in CA1.

Finally, we investigated whether this variable circuitry contributed to an observed variance in the globally recorded contralateral EEG signal. We observed a small but significant correlation (Pearson's $r = 0.13$, $P = 0.005$) between interictal spikes with correlated contralateral EEG signals and overlapping spatial imprints (Fig. 5F). Spikes with a low correlation of contralateral EEG signals were unlikely to show high spatial overlap, but the results were more variable for spikes with higher correlations between contralateral EEG signals. Some of this ambiguity could be due to the difficulty in assessing similarity when taking into account the fine dendritic structure in spatial imprints, and further work should investigate how specific GABAergic cell populations shape the electrophysiological correlates of interictal events. Regardless, this analysis demonstrates that the local variability in microcircuit recruitment reflected in the spatial patterning of calcium signals

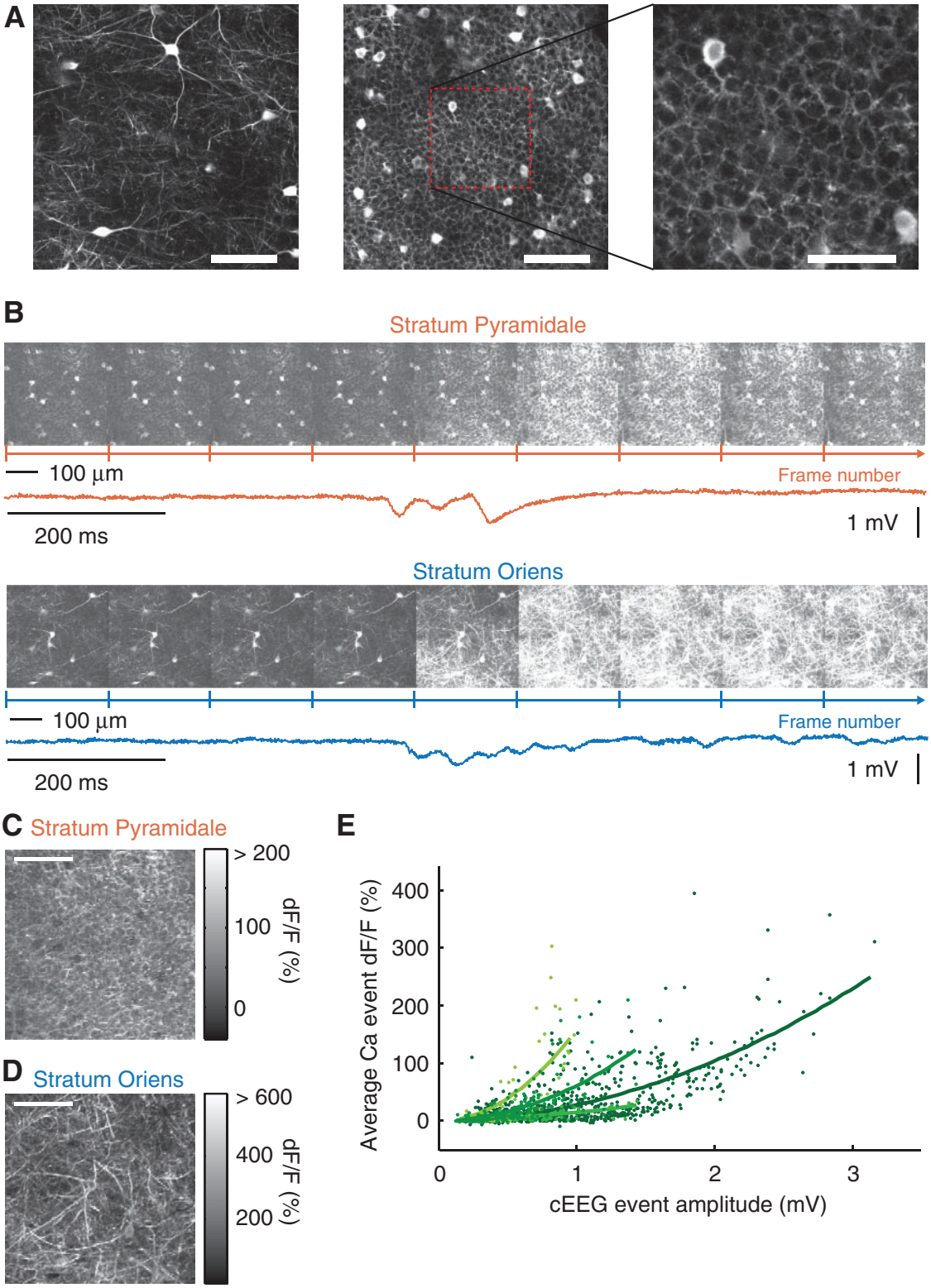

Figure 4 Calcium imaging of CA1 GABAergic neuron activity in GAD67-Cre mice. (**A**) Image of GCaMP5 signal in GABAergic cells from the stratum oriens (*left*, Scale bar = 100 µm) and stratum pyramidale (*middle*, Scale bar = 100 µm; *right*, Scale bar = 50 µm). (**B**) Successive movie frames showing GCaMP fluorescence signal from GABAergic cells and corresponding contralateral EEG signal for an interictal spike spike in the stratum pyramidale (orange, Supplementary Video 4) and stratum oriens (blue, Supplementary Video 5). (**C** and **D**) Corresponding spatial imprint of recruitment of GABAergic neurons during an interictal spike in the stratum pyramidale (**C**) and stratum oriens (**D**). Scale bar = 100 µm. (**E**) Relationship between the amplitude of the contralateral EEG and the average image dF/F during interictal spikes (same as Fig. 2D for wild-type mice, *n* = 4 mice, 1223 interictal spikes). Data from the stratum pyramidale and stratum oriens are pooled as the relationship was independent of the imaging location.

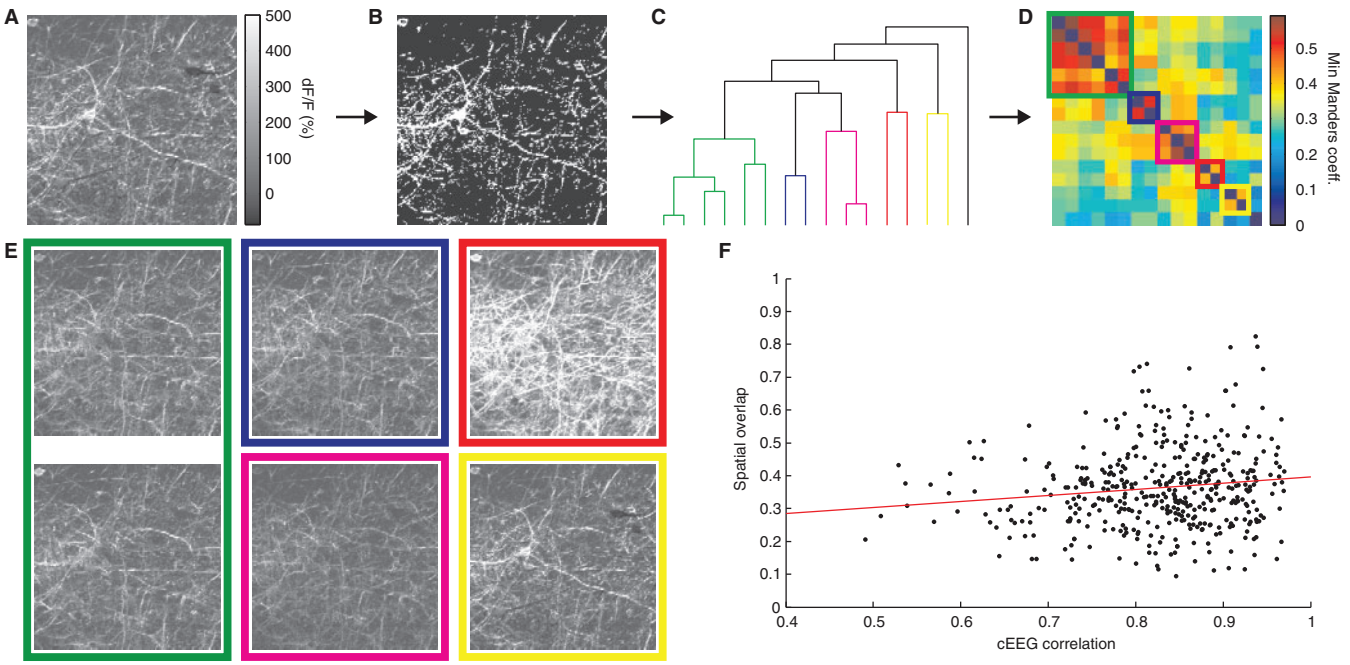

Figure 5 Spatial structure of GABAergic neuron recruitment. (**A**) Spatial imprint of an interictal spike imaged in the stratum oriens in a GAD67-Cre mouse. (**B**) Binarized version of the interictal spike in **A** showing spatial pattern of activated pixels. (**C**) Dendrogram resulting from average linkage hierarchical clustering of the similarity matrix between the spatial patterns of 16 interictal spikes from a single imaging session. (**D**) Similarity matrix sorted by the ordering from (**C**). Coloured boxes indicate observed community structure. (**E**) Examples of spatial imprints from the same community with similar spatial patterns (green) and interictal spikes with different patterns (from different communities; other coloured boxes). (**F**) Correlation between events with similar contralateral EEG during event and similar spatial structure (Pearson's r = 0.13, $P = 0.005$, $n = 436$ interictal spikes from four mice).

originating from GABAergic neurons shapes the macroscale epileptiform dynamics recorded globally.

Discussion

Here, for the first time, using two-photon calcium imaging in awake epileptic mice to probe CA1 multi-neuron dynamics with single-cell and axonal innervation resolution, we have shown that spontaneous interictal spikes recruit variable subsets of GABAergic neurons. In turn, their glutamatergic counterparts receive synchronous inhibitory input resulting from the activation of perisomatic GABAergic terminals, which reduces their firing rate, as revealed by the combined analysis of imaging and kCSD data. These results confirm previously reported increases of GABAergic transmission in various models of epilepsy (Chen *et al.*, 2001; Cossart *et al.*, 2001; Klaassen *et al.*, 2006) and theoretical predictions (Li *et al.*, 2008). Given that GABAergic neurons are a major substrate for cognitive function (Lewis, 2014), such imbalanced recruitment of inhibitory circuits, even outside of epileptogenic regions, could support the transitory or long-term cognitive impairments associated with interictal spiking (Binnie, 2003; Mosbah *et al.*, 2014). Future work should further investigate these potential links between GABAergic activation and cognitive deficits observed during interictal spiking.

Relationship to previous studies and clinical relevance

Synchronous GABAergic activity associated with epileptiform discharges has been previously reported in electrophysiological recordings from rodent acute slice models (Velazquez and Carlen, 1999; Zhang *et al.*, 2012), *in vivo* animal models (Prince, 1968), and resected human tissue (Cohen *et al.*, 2002; Huberfeld *et al.*, 2011). However, these previous studies involved reduced preparations that do not preserve network integrity and/or relied on convulsive agents (4-AP, low Mg^{2+}, high potassium, etc.) to artificially boost activity through a non-specific increase in neuronal excitability. Importantly, some of these agents (such as penicillin) have a direct action on GABAergic transmission which will likely impact cellular dynamics. In addition, previous studies analysed interictal-like events originating from normal functioning networks rather than from structurally and functionally rewired networks following epileptogenesis. The chronic experimental model studied here mimics the structural network changes reported in human patients after epileptogenesis (Curia *et al.*, 2008) and therefore is more likely to capture the relevant cellular mechanisms at the basis of epileptiform activity. The clinical translation of the synchronous activation of CA1 GABAergic neurons and resultant inhibition of principle cells observed here supports the hypothesis that

some interictal spikes in human patients may reflect a protective phenomenon (Avoli *et al*., 2013).

In studies that have previously described an increase in inhibitory drive, this increase was generally followed or paralleled by an increase in the excitatory drive, sometimes resulting from a direct depolarizing action of GABA in pathological tissue (Cohen *et al*., 2002). However, we do not observe this phenomenon because the activation of somatic GABAergic terminals does not induce spiking. We cannot exclude the possibility that glutamatergic activity is also contributing to the observed interictal spikes, but we do show that the synaptic inputs that potentially drive GABAergic neurons are not likely to originate from a burst of action potentials generated at the soma of local glutamatergic neurons since these neurons become quiescent during interictal spikes (although see 'Technical considerations' section below). In contrast, bursting activity is observed in principal layer neurons outside of interictal spikes, for example when the mouse is running on the treadmill.

We also provided the first *in vivo* demonstration with cellular resolution of the variability in neuronal recruitment during interictal events, a feature previously observed in slice recordings (Sabolek *et al*., 2012; Feldt Muldoon *et al*., 2013). Interestingly, both variability in neuronal recruitment as well as an increase in the inhibitory drive were also shown to be characteristic features of the so-called 'ictal penumbra' (Prince and Wilder, 1967; Dichter and Spencer, 1969*a*, *b*; Trevelyan *et al*., 2006; Trevelyan, 2009; Sabolek *et al*., 2012; Schevon *et al*., 2012; Trevelyan and Schevon, 2013), a region around the territory supporting ictal activity that displays large amplitude EEG signals, reflecting feedforward synaptic currents, but with little actual local recruitment of neurons. The presence of an ictal penumbra suggests heterogeneity in neuronal activation with massive activation only at certain spatially focused sites. It is possible that our data reflect a similar phenomenon, however, the previous work studying penumbral regions was done in regard to ictal events and the interictal spikes observed here are very likely to involve different mechanisms of neuronal recruitment than those which lead to seizures.

This finding also has potential implications regarding the interpretation of functional MRI data obtained from epileptic patients. It is likely that the magnitude of the contribution of GABAergic neurons to the blood oxygen level-dependent signal differs from that of excitatory cells (Buzsaki *et al*., 2007), and therefore one must be cautious when drawing conclusions about epileptiform activity when using this standard modality.

Technical considerations

As this study pushes current *in vivo* imaging techniques to their experimental limits, it is important to take some technical considerations into account when interpreting the data. First, to image at the depth of the dorsal hippocampus, it was necessary to remove a small portion of the overlying neocortex. While this could affect the propagation of interictal spikes through the neocortex, it is important to note that the interictal spikes detected in the contralateral EEG signal showed similar properties to those from previously studied TLE mice chronically implanted with a telemetric surface EEG (Feldt Muldoon *et al*., 2013). Additionally, the linear probe experiments presented here did not involve the removal of the neocortex, and we observed the same variation in spike shape, along with a silencing of neuronal activity in the stratum pyramidale and a current source that could represent the synchronous inflow of chloride into somata resulting from synchronous GABAergic inputs. Thus, the findings from the linear probe experiments in which the cortex was not removed are consistent with the data obtained in the imaging experiments that did involve the removal of a small portion of the cortex, supporting the notion that the removal of the cortex did not greatly influence the propagation dynamics. We also note that the pilocarpine model used in this study is a multifocal model and we have no reason to suspect that one hemisphere would preferentially be associated with the focus of spikes. Although interictal spike detection was done on the contralateral side, for all detected spikes, the linear probe recordings confirmed the presence of an associated ipsilateral spike.

Another important consideration stems from the fact that the exact firing patterns of CA1 pyramidal cells during interictal spikes are difficult to assess. The sharp slope associated with interictal spikes in linear probe recordings meant that a short window of time centred on the interictal spike had to be excluded from multiunit analysis. Thus, to examine cellular participation of cells in the stratum pyramidale during interictal spikes, we turned to imaging of calcium dynamics using GCaMP. These reporters are particularly well suited for our experimental conditions since they reliably detect bursting dynamics and 'epileptic' neurons have been shown to display a higher bursting propensity (Yaari and Beck, 2002). In principle, the ability of the GCaMP reporters to detect the influx of calcium from a single action potential is less reliable. For this reason, we used both GCaMP 5 and 6 variants as the newer GCaMP6 has been shown to be more sensitive to the detection of single action potentials, both in pyramidal cells and in interneurons (Chen *et al*., 2013). While we were able to detect more active cells in mice injected with GCaMP6 versus GCaMP5 (Supplementary material), these cells were observed to be active outside of interictal spikes, and the cellular recruitment in the stratum pyramidale during interictal spikes was not significantly different when using the two indicators. In addition, we have both directly and indirectly demonstrated the sensitivity of the GCaMP reporters to detect single spikes by performing juxtacellular spike recordings from single imaged neurons in anaesthetized mice, and by imaging ripple events in the stratum pyramidale. Still, it is possible that we failed to observe the activation of some cells in the stratum

pyramidale, especially those that display a tonic mode of firing for which two consecutive spikes are below our temporal resolution or cells that fire only a single action potential during the interictal spike.

Finally, it should be noted that we attempted to isolate the calcium signal originating only from pyramidal cells by performing calcium imaging, but could not find experimental conditions for which GCaMP expression was strictly restricted to glutamatergic neurons, as a small percentage of GABAergic cells additionally expressed the GCaMP indicator when using a CAMKII-Cre viral vector, and Emx1-Cre mice could no longer drive Cre expression in CA1 at adult stages.

Circuit mechanisms for the initiation and propagation of GABAergic activity

From a circuits perspective, our study introduces many questions. What are the upstream cellular mechanisms that support the preferential recruitment of GABAergic neurons? Are specific GABAergic microcircuits activated that contribute to the control of downstream neuronal populations? As mentioned above, the somata of most neurons located in the principal cell layer do not display spontaneous calcium transients during interictal spikes, but instead show decreased spiking as observed in multiunit extracellular recordings. It is therefore unlikely that GABAergic neurons are synaptically activated from local CA1 collateral inputs. However, it was previously reported that CA1 GABAergic neurons that were spared in the course of epileptogenesis (including those with perisomatic projections) received an enhanced glutamatergic drive that contributed to increased spontaneous firing (Cossart *et al.*, 2001). It was thought that this enhanced glutamatergic drive originated from the sprouting of local CA1 axon collaterals (Esclapez *et al.*, 1999; Cossart *et al.*, 2001). However, it may instead be that this arises from CA3 or the entorhinal cortex, as both regions provide a main excitatory drive to CA1 and were shown to be potential sites of origin for epileptiform events (Wozny *et al.*, 2005). In fact, rather than Schaffer collaterals from CA3, inputs originating from the entorhinal cortex were recently shown to be more likely to drive CA1 interneurons (as opposed to their glutamatergic counterparts) (Sun *et al.*, 2014). Additionally, it could be that glutamate is released due to distal axonal firing that occurs independently from somatic activity (Dugladze *et al.*, 2012). Alternatively, CA1 GABAergic neurons could be driven by a very sparse and currently unidentified population of glutamatergic bursting neurons (Miles and Wong, 1983; Marissal *et al.*, 2012), so we cannot exclude that GABAergic neurons could be driven by the few cells in the stratum pyramidale that are detected as being active during interictal spikes. Finally, the preferential activation of interneurons may result from several other factors, including a lower action potential threshold, short response latency, and fast axonal signalling (Geiger *et al.*, 1997; Galarreta and Hestrin, 2001; Hu *et al.*, 2010; Hu and Jonas, 2014), the properties and distribution of the excitatory synapses they receive (in particular higher amplitude excitatory postsynaptic potentials) (Gulyas *et al.*, 1999; Megias *et al.*, 2001; Molnar *et al.*, 2008), or their forming a gap-junction syncytium (Galarreta and Hestrin, 1999; Gigout *et al.*, 2006). Thus, future work is needed to identify the upstream source of GABAergic cell coordination.

Identification of the specific downstream targets of GABAergic neurons recruited during interictal spikes is also an important issue due to the critical role that subsets of GABAergic neurons play in single-handedly priming network bursts and behaviour (Bonifazi *et al.*, 2009; Ellender *et al.*, 2010; Doron *et al.*, 2014), and the fact that there is increasing experimental evidence indicating that inhibition can balance and even oppose spreading excitatory activity very effectively (Prince and Wilder, 1967; Grenier *et al.*, 2001, 2003; Timofeev *et al.*, 2002; Trevelyan *et al.*, 2006; Rheims *et al.*, 2008). Given that the cellular recruitment we describe is heterogeneous, it is likely that, in addition to perisomatic projecting neurons, other classes of GABAergic neurons are also recruited during interictal spikes. For example, the activation of somata in the pyramidal layer could be observed when imaging GAD67-Cre mice, which suggests that GABAergic neurons in that layer, i.e. basket cells and Ivy cells (Fuentealba *et al.*, 2008), could be recruited. In fact they represent a similar fraction to the fraction cells detected as being active in the stratum pyramidale during interictal spikes (Supplementary Fig. 2). Interestingly, an additional sprouting of GABAergic axons has recently been revealed, which could also link CA1 to the dentate gyrus and have important functional consequences in the present context (Peng *et al.*, 2013).

Linking micro and macroscopic scales

Finally, it is important to understand the relationship between micro and macro network activity because the various mechanisms proposed to underlie the generation of epileptiform discharges are united by the assumption that their dynamics are conserved across multiple scales. A somewhat unexpected finding of this study is the correlation between the maximum value of the kCSD source located in the pyramidal layer and the amplitude of interictal spikes recorded at the global/surface level from the contralateral EEG. Additionally, we found a supralinear relationship between the amplitude of the locally observed cellular GCaMP fluorescence signal and the contralateral EEG amplitude of interictal spikes. Notably, this relationship was independent of the depth of imaging. Given that we also observed variable spatial patterning as different subsets of GABAergic cells were recruited during sequential interictal spikes, it is unlikely that this supralinear response is solely due to a progressive increase in the number of cells recruited during spikes. In fact, it has been shown that the

relationship between the number of action potentials fired and the fluorescence amplitude of the GCaMP indicator is also supralinear (Akerboom *et al.*, 2012; Chen *et al.*, 2013). This suggests that the amplitude of the interictal spike, measured at the macroscopic scale, could reflect an increased firing rate of cells that are recruited in our microscopic imaging area. Whether or not this reflects a globally observed phenomenon throughout all brain regions or if the global signal is dominated by the GABAergic activity we observe locally remains an open question (Trevelyan, 2009; Bazelot *et al.*, 2010).

We also observed a small but significant relationship between interictal spikes with similar spatial patterning and spike shape, with the main observation being that spikes with a lower correlation between contralateral EEG shapes were unlikely to also have similar spatial patterning of cellular recruitment. Spikes with a high correlation of contralateral EEG shape displayed a more variable relationship between spatial patterning of interictal spikes. However, because of the difficulty in comparing images of the fine dendritic webs recruited during interictal spikes (even after movement correction of images, small shifts of a few pixels in dendritic location matter when comparing spatial patterns of recruitment), it is likely that our analysis underestimated this relationship. Therefore, future studies should additionally address cellular recruitment in different areas and how different brain regions and neuronal subpopulations differentially contribute to the globally measured EEG signals observed at the surface of the brain.

In conclusion, our finding that inhibitory GABAergic microcircuits are the main participants of interictal activity in CA1 supports recent theoretical and experimental predictions by connecting several separate pieces of previous evidence supporting the importance of GABAergic inhibition in shaping epileptiform activity. Importantly, we also provided the first demonstration of these principles in the intact brain of un-anaesthetized chronically epileptic animals, which is a modality that has not been previously explored. This work therefore provides valuable insight into the micro-scale epileptiform dynamics that underlie macro-scale subdural EEG signals, and suggests that large scale inhibition could potentially be related to some of the clinically observed cognitive deficits associated with interictal spikes.

Acknowledgements

We acknowledge the GENIE Program and the Janelia Farm Research Campus, specifically for GCAMP5G: Loren L. Looger, Ph.D., Jasper Akerboom, Ph.D., Douglas S. Kim, Ph.D and for GCAMP6m: Vivek Jayaraman, Ph.D., Rex A. Kerr, Ph.D., Douglas S. Kim, Ph.D., Loren L. Looger, Ph.D., Karel Svoboda, Ph.D. from the GENIE Project, Janelia Farm Research Campus, Howard Hughes Medical Institute. We also thank Daniel Wójcik for helpful comments and providing the Matlab code used in the kCSD analysis, Pr. Hannah Monyer for providing the GAD67-Cre mice, Pr. Daniel Dombeck for helping with the implantation of the chronic hippocampal imaging window and Drs E. Andresen and L. Gallais for designing the window for juxtacellular recordings.

Funding

We acknowledge funding from an FP7-PEOPLE-2011-IIF Marie Curie Fellowship (#301728 S.F.M.), an FP7-ERC 'GABA Networks' grant (#242842; V.V., T.T., R.C.), the Fondation pour la Recherche Medicale (R.C.), and an ERA-Net: EpiNet Grant (V.V., R.C.).

Supplementary material

Supplementary material is available at Brain online.

References

Akerboom J, Chen TW, Wardill TJ, Tian L, Marvin JS, Mutlu S, et al. Optimization of a GCaMP calcium indicator for neural activity imaging. J Neurosci 2012; 32: 13819–40.

Alvarado-Rojas C, Lehongre K, Bagdasaryan J, Bragin A, Staba R, Engel J, Jr, et al. Single-unit activities during epileptic discharges in the human hippocampal formation. Front Comput Neurosci 2013; 7: 140.

Ang CW, Carlson GC, Coulter DA. Massive and specific dysregulation of direct cortical input to the hippocampus in temporal lobe epilepsy. J Neurosci 2006; 26: 11850–6.

Avoli M, de Curtis CM. GABAergic synchronization in the limbic system and its role in the generation of epileptiform activity. Prog Neurobiol 2011; 95: 104–32.

Avoli M, de Curtis CM, Kohling R. Does interictal synchronization influence ictogenesis? Neuropharmacology 2013; 69: 37–44.

Badier JM, Chauvel P. Spatio-temporal characteristics of paroxysmal interictal events in human temporal lobe epilepsy. J Physiol Paris 1995; 89: 255–64.

Bazelot M, Dinocourt C, Cohen I, Miles R. Unitary inhibitory field potentials in the CA3 region of rat hippocampus. J Physiol 2010; 588: 2077–90.

Bernard C, Anderson A, Becker A, Poolos NP, Beck H, Johnston D. Acquired dendritic channelopathy in temporal lobe epilepsy. Science 2004; 305: 532–5.

Binnie CD. Cognitive impairment during epileptiform discharges: is it ever justifiable to treat the EEG? Lancet Neurol 2003; 2: 725–30.

Blume WT, Holloway GM, Wiebe S. Temporal epileptogenesis: localizing value of scalp and subdural interictal and ictal EEG data. Epilepsia 2001; 42: 508–14.

Bonifazi P, Goldin M, Picardo MA, Jorquera I, Cattani A, Bianconi G, et al. GABAergic hub neurons orchestrate synchrony in developing hippocampal networks. Science 2009; 326: 1419–24.

Bourien J, Bartolomei F, Bellanger JJ, Gavaret M, Chauvel P, Wendling F. A method to identify reproducible subsets of co-activated structures during interictal spikes. Application to intracerebral EEG in temporal lobe epilepsy. Clin Neurophysiol 2005; 116: 443–55.

Brooks-Kayal AR, Shumate MD, Jin H, Rikhter TY, Coulter DA. Selective changes in single cell GABA(A) receptor subunit expression and function in temporal lobe epilepsy [see comments]. Nat Med 1998; 4: 1166–72.

Buzsaki G, Anastassiou CA, Koch C. The origin of extracellular fields and currents–EEG, ECoG, LFP and spikes. Nat Rev Neurosci 2012; 13: 407–20.

Buzsaki G, Hsu M, Slamka C, Gage FH, Horvath Z. Emergence and propagation of interictal spikes in the subcortically denervated hippocampus. Hippocampus 1991; 1: 163–80.
Buzsaki G, Kaila K, Raichle M. Inhibition and brain work. Neuron 2007; 56: 771–83.
Cavalheiro EA, Santos NF, Priel MR. The pilocarpine model of epilepsy in mice. Epilepsia 1996; 37: 1015–19.
Chagnac-Amitai Y, Connors BW. Horizontal spread of synchronized activity in neocortex and its control by GABA-mediated inhibition. J Neurophysiol 1989; 61: 747–58.
Chauviere L, Doublet T, Ghestem A, Siyoucef SS, Wendling F, Huys R, et al. Changes in interictal spike features precede the onset of temporal lobe epilepsy. Ann Neurol 2012; 71: 805–14.
Chen K, Aradi I, Thon N, Eghbal-Ahmadi M, Baram TZ, Soltesz I. Persistently modified h-channels after complex febrile seizures convert the seizure-induced enhancement of inhibition to hyperexcitability. Nat Med 2001; 7: 331–37.
Chen TW, Wardill TJ, Sun Y, Pulver SR, Renninger SL, Baohan A, et al. Ultrasensitive fluorescent proteins for imaging neuronal activity. Nature 2013; 499: 295–300.
Cohen I, Navarro V, Clemenceau S, Baulac M, Miles R. On the origin of interictal activity in human temporal lobe epilepsy *in vitro*. Science 2002; 298: 1418–21.
Cossart R, Bernard C, Ben-Ari Y. Multiple facets of GABAergic neurons and synapses: multiple fates of GABA signalling in epilepsies. Trends Neurosci 2005; 28: 108–15.
Cossart R, Dinocourt C, Hirsch JC, Merchan-Perez A, De Felipe J, Ben-Ari Y, et al. Dendritic but not somatic GABAergic inhibition is decreased in experimental epilepsy. Nat Neurosci 2001; 4: 52–62.
Csicsvari J, Hirase H, Czurko A, Mamiya A, Buzsaki G. Fast network oscillations in the hippocampal CA1 region of the behaving rat. J Neurosci 1999; 19: RC20.
Curia G, Longo D, Biagini G, Jones RS, Avoli M. The pilocarpine model of temporal lobe epilepsy. J Neurosci Methods 2008; 172: 143–57.
de Curtis M, Avanzini G. Interictal spikes in focal epileptogenesis. Prog Neurobiol 2001; 63: 541–67.
Dichter M, Spencer WA. Penicillin-induced interictal discharges from the cat hippocampus. I. Characteristics and topographical features. J Neurophysiol 1969a; 32: 649–62.
Dichter M, Spencer WA. Penicillin-induced interictal discharges from the cat hippocampus. II. Mechanisms underlying origin and restriction. J Neurophysiol 1969b; 32: 663–87.
Dombeck DA, Harvey CD, Tian L, Looger LL, Tank DW. Functional imaging of hippocampal place cells at cellular resolution during virtual navigation. Nat Neurosci 2010; 13: 1433–40.
Doron G, von HM, Schlattmann P, Houweling AR, Brecht M. Spiking irregularity and frequency modulate the behavioral report of single-neuron stimulation. Neuron 2014; 81: 653–63.
Dugladze T, Schmitz D, Whittington MA, Vida I, Gloveli T. Segregation of axonal and somatic activity during fast network oscillations. Science 2012; 336: 1458–61.
Ellender TJ, Nissen W, Colgin LL, Mann EO, Paulsen O. Priming of hippocampal population bursts by individual perisomatic-targeting interneurons. J Neurosci 2010; 30: 5979–91.
Esclapez M, Hirsch JC, Ben-Ari Y, Bernard C. Newly formed excitatory pathways provide a substrate for hyperexcitability in experimental temporal lobe epilepsy. J Comp Neurol 1999; 408: 449–60.
Fabene PF, Navarro MG, Martinello M, Martinello M, Rossi B, Merigo F, et al. A role for leukocyte-endothelial adhesion mechanisms in epilepsy. Nat Med 2008; 14: 1377–83.
Feldt Muldoon S, Soltesz I, Cossart R. Spatially clustered neuronal assemblies comprise the microstructure of synchrony in chronically epileptic networks. Proc Natl Acad Sci USA 2013; 110: 3567–72.
Fuentealba P, Begum R, Capogna M, Jinno S, Márton LF, Csicsvari J, et al. Ivy cells: a population of nitric-oxide-producing, slow-spiking GABAergic neurons and their involvement in hippocampal network activity. Neuron 2008; 57: 917–29.
Galarreta M, Hestrin S. A network of fast-spiking cells in the neocortex connected by electrical synapses. Nature 1999; 402: 72–5.
Galarreta M, Hestrin S. Electrical synapses between GABA-releasing interneurons. Nat Rev Neurosci 2001; 2: 425–33.
Geiger JR, Lubke J, Roth A, Frotscher M, Jonas P. Submillisecond AMPA receptor-mediated signaling at a principal neuron- interneuron synapse. Neuron 1997; 18: 1009–23.
Gibbs FA, Davis H, Lennox WG. The electroencephalogram in epilepsy and conditions with impaired consciousness. Arch Neurol Psychiatry 1935; 34: 1133–48.
Gigout S, Louvel J, Kawasaki H, D'Antuono M, Armand V, Kurcewicz I, et al. Effects of gap junction blockers on human neocortical synchronization. Neurobiol Dis 2006; 22: 496–508.
Greenberg DS, Houweling AR, Kerr JN. Population imaging of ongoing neuronal activity in the visual cortex of awake rats. Nat Neurosci 2008; 11: 749–51.
Grenier F, Timofeev I, Steriade M. Focal synchronization of ripples (80-200 Hz) in neocortex and their neuronal correlates. J Neurophysiol 2001; 86: 1884–98.
Grenier F, Timofeev I, Steriade M. Neocortical very fast oscillations (ripples, 80-200 Hz) during seizures: intracellular correlates. J Neurophysiol 2003; 89: 841–52.
Gulyas AI, Freund TT. Generation of physiological and pathological high frequency oscillations: the role of perisomatic inhibition in sharp-wave ripple and interictal spike generation. Curr Opin Neurobiol 2014; 31C: 26–32.
Gulyas AI, Megias M, Emri Z, Freund TF. Total number and ratio of excitatory and inhibitory synapses converging onto single interneurons of different types in the CA1 area of the rat hippocampus. J Neurosci 1999; 19: 10082–97.
Hu H, Jonas P. A supercritical density of Na(+) channels ensures fast signaling in GABAergic interneuron axons. Nat Neurosci 2014; 17: 686–93.
Hu H, Martina M, Jonas P. Dendritic mechanisms underlying rapid synaptic activation of fast-spiking hippocampal interneurons. Science 2010; 327: 52–8.
Huberfeld G, Menendez de la PL, Pallud J, Cohen I, Le Van Quyen M, Adam C, et al. Glutamatergic pre-ictal discharges emerge at the transition to seizure in human epilepsy. Nat Neurosci 2011; 14: 627–34.
Huneau C, Benquet P, Dieuset G, Biraben A, Martin B, Wendling F. Shape features of epileptic spikes are a marker of epileptogenesis in mice. Epilepsia 2013; 54: 2219–27.
Hunt RF, Girskis KM, Rubenstein JL, Alvarez-Buylla A, Baraban SC. GABA progenitors grafted into the adult epileptic brain control seizures and abnormal behavior. Nat Neurosci 2013; 16: 692–7.
Keller CJ, Truccolo W, Gale JT, Eskandar E, Thesen T, Carlson C, et al. Heterogeneous neuronal firing patterns during interictal epileptiform discharges in the human cortex. Brain 2010; 133: 1668–81.
Klaassen A, Glykys J, Maguire J, Labarca C, Mody I, Boulter J. Seizures and enhanced cortical GABAergic inhibition in two mouse models of human autosomal dominant nocturnal frontal lobe epilepsy. Proc Natl Acad Sci USA 2006; 103: 19152–7.
Krook-Magnuson E, Armstrong C, Oijala M, Soltesz I. On-demand optogenetic control of spontaneous seizures in temporal lobe epilepsy. Nat Commun 2013; 4: 1376.
Lewis DA. Inhibitory neurons in human cortical circuits: substrate for cognitive dysfunction in schizophrenia. Curr Opin Neurobiol 2014; 26C: 22–6.
Li Y, Fleming IN, Colpan ME, Mogul DJ. Neuronal desynchronization as a trigger for seizure generation. IEEE Trans Neural Syst Rehabil Eng 2008; 16: 62–73.
Lovett-Barron M, Kaifosh P, Kheirbek MA, Danielson N, Zaremba JD, Reardon TR, et al. Dendritic inhibition in the hippocampus supports fear learning. Science 2014; 343: 857–63.

Marchionni I, Maccaferri G. Quantitative dynamics and spatial profile of perisomatic GABAergic input during epileptiform synchronization in the CA1 hippocampus. J Physiol 2009; 587: 5691–708.
Marissal T, Bonifazi P, Picardo MA, Nardou R, Petit LF, Baude A, et al. Pioneer glutamatergic cells develop into a morpho-functionally distinct population in the juvenile CA3 hippocampus. Nat Commun 2012; 3: 1316.
Megias M, Emri Z, Freund TF, Gulyas AI. Total number and distribution of inhibitory and excitatory synapses on hippocampal CA1 pyramidal cells. Neuroscience 2001; 102: 527–40.
Melzer S, Michael M, Caputi A, Eliava M, Fuchs EC, Whittington MA, et al. Long-range-projecting GABAergic neurons modulate inhibition in hippocampus and entorhinal cortex. Science 2012; 335: 1506–10.
Miles R, Wong R. Single neurons can initiate synchronized population discharge in the hippocampus. Nature 1983; 306: 371–3.
Molnar G, Olah S, Komlosi G, Füle M, Szabadics J, Varga C, et al. Complex events initiated by individual spikes in the human cerebral cortex. PLoS Biol 2008; 6: e222.
Mosbah A, Tramoni E, Guedj E, Aubert S, Daquin G, Ceccaldi M, et al. Clinical, neuropsychological, and metabolic characteristics of transient epileptic amnesia syndrome. Epilepsia 2014; 55: 699–706.
Nusser Z, Cull-Candy S, Farrant M, Hausser M, Clark BA. Differences in synaptic GABA(A) receptor number underlie variation in GABA mini amplitude Tonic synaptic inhibition modulates neuronal output pattern and spatiotemporal synaptic integration. Neuron 1997; 19: 665–78.
Peng Z, Zhang N, Wei W, Huang CS, Cetina Y, Otis TS, et al. A reorganized GABAergic circuit in a model of epilepsy: evidence from optogenetic labeling and stimulation of somatostatin interneurons. J Neurosci 2013; 33: 14392–405.
Potworowski J, Jakuczun W, Leski S, Wojcik D. Kernel current source density method. Neural Computation 2012; 24: 541–75.
Prince DA. Inhibition in "epileptic" neurons. Exp Neurol 1968; 21: 307–21.
Prince DA, Wilder BJ. Control mechanisms in cortical epileptogenic foci. "Surround" inhibition. Arch Neurol 1967; 16: 194–202.
Rheims S, Represa A, Ben-Ari Y, Zilberter Y. Layer-specific generation and propagation of seizures in slices of developing neocortex: role of excitatory GABAergic synapses. J Neurophysiol 2008; 100: 620–8.
Royer S, Zemelman BV, Losonczy A, Kim J, Chance F, Magee JC, et al. Control of timing, rate and bursts of hippocampal place cells by dendritic and somatic inhibition. Nat Neurosci 2012; 15: 769–75.
Sabolek HR, Swiercz WB, Lillis KP, Cash SS, Huberfeld G, Zhao G, et al. A candidate mechanism underlying the variance of interictal spike propagation. J Neurosci 2012; 32: 3009–21.
Schevon CA, Weiss SA, McKhann G, Jr, Goodman RR, Yuste R, Emerson RG, et al. Evidence of an inhibitory restraint of seizure activity in humans. Nat Commun 2012; 3: 1060.
Smolders I, Bortolotto ZA, Clarke VR, Warre R, Khan GM, O'Neill MJ, et al. Antagonists of GLU(K5)-containing kainate receptors prevent pilocarpine-induced limbic seizures. Nat Neurosci 2002; 5: 796–804.
Staley KJ, White A, Dudek FE. Interictal spikes: harbingers or causes of epilepsy? Neurosci Lett 2011; 497: 247–50.
Sun Y, Nguyen AQ, Nguyen JP, Le L, Saur D, Choi J, et al. Cell-type-specific circuit connectivity of hippocampal CA1 revealed through Cre-dependent rabies tracing. Cell Rep 2014; 7: 269–80.
Timofeev I, Grenier F, Steriade M. The role of chloride-dependent inhibition and the activity of fast-spiking neurons during cortical spike-wave electrographic seizures. Neuroscience 2002; 114: 1115–32.
Tolu S, Avale ME, Nakatani H, Pons S, Parnaudeau S, Tronche F, et al. A versatile system for the neuronal subtype specific expression of lentiviral vectors. FASEB J 2010; 24: 723–30.
Trevelyan AJ. The direct relationship between inhibitory currents and local field potentials. J Neurosci 2009; 29: 15299–307.
Trevelyan AJ, Schevon CA. How inhibition influences seizure propagation. Neuropharmacology 2013; 69: 45–54.
Trevelyan AJ, Sussillo D, Watson BO, Yuste R. Modular propagation of epileptiform activity: evidence for an inhibitory veto in neocortex. J Neurosci 2006; 26: 12447–55.
Truccolo W, Donoghue JA, Hochberg LR, Eskandar EN, Madsen JR, Anderson WS, et al. Single-neuron dynamics in human focal epilepsy. Nat Neurosci 2011; 14: 635–41.
Velazquez JL, Carlen PL. Synchronization of GABAergic interneuronal networks during seizure-like activity in the rat horizontal hippocampal slice. Eur J Neurosci 1999; 11: 4110–18.
Wozny C, Gabriel S, Jandova K, Schulze K, Heinemann U, Behr J. Entorhinal cortex entrains epileptiform activity in CA1 in pilocarpine-treated rats. Neurobiol Dis 2005; 19: 451–60.
Wozny C, Kivi A, Lehmann TN, Dehnicke C, Heinemann U, Behr J. Comment on "On the origin of interictal activity in human temporal lobe epilepsy *in vitro*". Science 2003; 301: 463.
Yaari Y, Beck H. "Epileptic neurons" in temporal lobe epilepsy. Brain Pathol 2002; 12: 234–9.
Zhang ZJ, Koifman J, Shin DS, Ye H, Florez CM, Zhang L, et al. Transition to seizure: ictal discharge is preceded by exhausted presynaptic GABA release in the hippocampal CA3 region. J Neurosci 2012; 32: 2499–512.
Zhou JL, Lenck-Santini PP, Zhao Q, Holmes GL. Effect of interictal spikes on single-cell firing patterns in the hippocampus. Epilepsia 2007; 48: 720–31.

Supplementary Materials and Methods

Pilocarpine model of temporal lobe epilepsy (TLE)

Adult mice (P31-P57) were first given injections of scopolamine methyl nitrate (1 mg/kg, i.p.), followed 20-30 minutes later by an injection of pilocarpine (330-350 mg/kg, i.p.) as in (Feldt Muldoon *et al.*, 2013). Animals were continuously observed to identify the onset of status epilepticus (SE). Mice that did not enter SE within 1 hour of the initial injection of pilocarpine were given an additional half dose of pilocarpine to induce SE and mice that did not enter SE were not used for experiments. Mice received diazepam (10 mg/kg, i.p.) 60 minutes after the onset of SE, and this injection was repeated as needed to help terminate seizures. Mice were given water-soaked food and allowed to recover for at least one week (range 7-120 days) before injections of viral vectors. Based on previous experience in the lab using telemetric EEG to monitor pilocarpine treated mice, 96 % of mice (n = 24/25) reached the chronic phase (development of spontaneous seizures) within 26 days and 100 % of pilocarpine treated mice reached the chronic phase within 35 days (TLE mice). Therefore, we waited an average of 58 ± 11 days (range 26-136) between pilocarpine injections and the first recording session to ensure that the mice had reached the chronic phase of the model.

GCaMP injections

In order to perform large-scale calcium imaging, wild type TLE mice were injected with a viral solution (titer: ~10^{12} genomes copy/ml; Penn Vector Core) of either AAV2/1.Syn.GCaMP5G (GCaMP3-T302L.R303P.D380Y).WPRE.SV40 (n = 3), AAV2/1.Syn.GCaMP6m.WPRE.SV40 (n = 3), or TLE GAD67-Cre mice with AAV2/1.hSynap.Flex.GCaMP5G (GCaMP3-T302L.R303P.D380Y).WPRE.SV40 (n = 4). Mice were first anesthetized (100 mg /kg ketamine, 10 mg /kg xylazine), and 500nl of viral solution was injected at a rate of 100 nL/min into the left dorsal hippocampus at following coordinates: AP: 2 & 2.5; ML: 1.6 & 2.1 relative to bregma; DV: 1.3 relative to brain surface. The constrained tissue was allowed to recover for one minute prior and three minutes after injections to prevent injection backwash. Mice were allowed to recover for a minimum of 7 days before the implantation of chronic electrodes.

Histological characterization of GCaMP5G expression

Viruses were injected as previously described and mice were perfused 16 days after virus injection (ANTIGENEFIX, DIAPATH). Twenty-four hours post fixation, 50 µm coronal slices were processed. After a pre-incubation in 5% normal donkey serum, sections were incubated overnight in primary antibodies (rabbit anti-GFAP, 1/2000 or mouse anti-NeuN, 1/500) diluted in PBS containing 0.3% triton X-100 (PBST). After washing in PBS, sections were incubated for 2 hours in appropriate secondary antibodies (1:500) conjugated with Cy3 (Jackson ImmunoResearch Laboratories) diluted in PBS. After washing, sections were mounted in Vectashield mounting media (Vector Laboratories Inc., Burlingame, CA, USA) between the slide and coverslip. Epifluorescent images were obtained with a Zeiss AxioImager Z2 microscope coupled to a camera (Zeiss AxioCam MR3). Immunofluorescence images were acquired using a HBO lamp associated with (470/40, 545/25) filter cubes for detection of non-amplified GCaMP5G and Cy3 signals. Confocal images were obtained with a Leica SP5-X spectral. *In vivo* images were acquired 3-8 days after the canula implantation (as performed for epileptic mice) using a two-photon microscope. Counts were performed manually using the Fiji cell counter plugin.

Implantation of chronic electrodes

For the implantation of chronic, contralateral electrodes, mice were anesthetized with ketamine (100 mg /kg) and xylazine (10 mg /kg). To record the global cortico-hippocampal electroencephalogram (cEEG) signal, a Jeweler's screw was implanted at AP: 3.7; ML: -3.7 relative to bregma. For the contralateral hippocampal local field potential (cLFP), a stainless steel Teflon coated wire was inserted in the contralateral hippocampus at following coordinates: AP: 2.5; ML: -2.5 relative to bregma; DV: 1.4 relative to the brain surface, and firmly fixed with Super-bond (DSM Dentaire). Neck electromyogram (EMG) recordings were obtained from a staple fastened to the neck muscle to provide a direct measure of the muscle tone. All electrodes were referenced relative to a Jeweler's screw inserted above the cerebellum and connectors were fixed with dental cement. Additionally, a metal bar was fixed at the back of the head to allow for head fixed recordings in a custom made restraint attached to a non-motorized linear

treadmill. For ipsilateral recordings, a small craniotomy (0.7mm diameter) was performed, centered at following coordinates: AP: 2.5; ML: -2.5 relative to bregma, and bone wax was applied to the hole. Mice were either allowed to recover and used for acute linear probe recordings (n = 4) or further implantation of a chronic imaging window was performed and mice were used for two-photon imaging experiments (n = 10).

Acute linear probe recordings

We used a 16-channel linear silicon probe (A1x16-5mm-25-177-A16, Neuronexus) to obtain acute recordings of the LFP depth profile of the CA1 region. We took advantage of the high density of recording sites (spacing 25µm) to precisely map local field potentials throughout the *stratum oriens*, *stratum pyramidale* and the top of the *stratum radiatum*, as well as to record multi-unit activity in the *stratum pyramidale*. Of the 16 channels, 3 were devoted to contralateral recordings (channels 11, 13, 15), meaning that the spacing of the deepest channels (1-10) was 25µm and 50 µm in the upper 3 channels (12, 14, 16). Mice with previously implanted chronic contralateral electrodes were head fixed, the wax covering craniotomy was gently removed, and the dura was opened. The probe was first coated with a DiI solution before being placed at the center of the craniotomy. The probe was gently lowered into the brain under electrophysiological control at a slow speed (< 25 µm/s) until deepest channels reached the *stratum pyramidale*. The lowering speed was reduced (< 10 µm/s) and the probe was further positioned such that the lower channels reached the *stratum radiatum*. The tissue was allowed to recover for 15 minutes before recordings began. Series of 5 minute recordings were made using a multi-channel recording system (Model 3600, AM-Systems) with 400X amplification, digitized at 50 kHz through a 1440A Digidata (Axon instrument), and visualized using Axoscope 10 software (Axon instrument). During recordings, mice were free to move on a non-motorized treadmill and experiments were done in the dark during the dark period of the light/dark cycle. The total head-fixed time did not exceed 4 hours, and mice were immediately perfused at the end of the recording period for histological confirmation of probe location.

Histology

Immediately after linear probe recordings, mice were anesthetized with ketamine (100 mg /kg) and xylazine (10 mg /kg) and transcardially perfused with 4% paraformaldehyde in phosphate buffer at a rate of ~4 ml/min. Brains were post-fixed overnight in fixative, washed in saline phosphate buffer (PBS), and sectioned coronally (100µm) with a vibratome (Leica VT1200 S). Slices were stained with DAPI (Sigma) and mounted on coverslips. Fluorescent images were obtained with a Zeiss AxioImager Z2 microscope (Carl Zeiss, Jena, Germany) coupled to a camera (AxioCam MR3). Acquisitions were done using a 10X objective (NA 0.3), and illumination was provided by a HXP lamp associated with DAPI (LP365; 395; 445/40) and Texas Red (560/40; 585; 630/75) filter cubes for DAPI and DiI detection respectively. The probe position was validated by measuring the deepest continuous DiI mark, and the channel located in the *stratum pyramidale* was identified for multiunit analysis of *stratum pyramidale* cells.

Interictal Spike detection

Interictal spikes were semi-automatically detected from the electrophysiological data simultaneously recorded in the contralateral hemisphere during imaging/probe recording sessions using custom made software written in Matlab. For mice used in probe recordings, the signals were first downsampled to 2 kHz to match the rate used for imaging recordings. To remove noise artifacts, cEEG and cLFP signals were filtered between 1 and 25 Hz using a fourth order Butterworth filter, and a moving standard deviation of the filtered signal was calculated over a 5 second sliding window. Potential spikes were selected as points where both the filtered cEEG and cLFP signals exceed a user defined threshold, generally 2-3 times the standard deviation. Potential spikes were then visually compared to the EMG signal to separate true spikes from movement artifacts, and the start and end times of the spike were manually marked using the unfiltered signal. This method biased our detection of interictal spikes to spikes that occurred outside of periods of large movement. The time of the spike was chosen to be the point of maximal deflection in the unfiltered signal and the spike amplitude was calculated was measured as the distance from the baseline (averaged over a 10 ms window before the start of each spike) to the point of maximum deflection. The spike

times extracted from the electrophysiological data were then aligned with the corresponding movie frames for further analysis.

kCSD Analysis

The spatial properties describing sinks and sources during interictal spikes were evaluated using the 13 channel LFPs from our linear probe recordings and a kernel source density method (kCSD, for further details see (Potworowski *et al.*, 2012)). This method of analysis does not assume even electrode spacing and was chosen due to the uneven spacing of the upper electrodes of our linear probe. Interictal spikes were detected as described above and the kCSD analysis was implemented in Matlab over a 200 ms window surrounding each spike. This analysis includes an optimization step to choose two of the parameters (the width of the basis elements and the regularization parameter). Since this calculation varied slightly from spike to spike, we examined the distribution of the optimal parameter for spikes from each mouse and then fixed the parameter to be equal to the mode of the distribution and re-ran the analysis. Thus, spikes within the same mouse were analyzed with the same set of parameters, but the optimization was allowed to vary between mice. Correlation between the spike amplitude and maximum value of the source was assessed using Spearman's rank correlation. In one mouse out of four used for the probe experiments, the recorded signal saturated the amplifier during the spikes so this mouse was discarded from the kCSD analysis. Additionally, in one other mouse, obvious movement artifacts occurred during 7 interictal spikes so these spikes were also removed from the analysis. This resulted in a final analysis of $n = 158$ interictal spikes recorded from 3 mice.

Multiunit detection

For the analysis of multiunit activity of putative pyramidal cells, the probe channel in which unit activity could be seen visually and was histologically verified to be located in the *stratum pyramidale* (see above) was selected for multiunit detection. In one mouse out of the four used, we could not detect unit activity in any of the recorded channels and thus this mouse was discarded from further analysis, meaning that the analysis was performed over $n = 131$ interictal spikes recorded from 3 mice. The signal

was first zero phase digitally filtered between 300 and 3000 Hz using a fourth order Butterworth filter. A baseline movement-free period of 10s was selected to be used as a baseline signal, and multiunit activity was detected as points in time where the signal exceeded a threshold of 5 times the standard deviation of the baseline signal. For the comparison of firing rates before and after interictal spikes, for each spike, the average firing rate was calculated for a 500 ms window immediately before and immediately after each spike. Distributions were compared using a two-sample t-test.

Implantation of chronic window for imaging experiments

This procedure was inspired from (Dombeck *et al.*, 2010) and adapted slightly for large-scale imaging. Briefly, mice were anesthetized with ketamine (100 mg /kg) and xylazine (10 mg /kg), chronic electrodes and a head restraint bar were implanted (see above), and a ~3mm diameter craniotomy centered over injection sites was performed. The dura was gently cut and a small portion of the cortex was aspirated to allow optical access to the hippocampus. The cortex was continuously irrigated to limit, prevent, and stop bleeding during cortex withdrawal. Similarly to the original method, the external capsule was exposed and allowed to dry until tacky, upon which a stainless steel canula (Microgroup) attached to a glass coverslip was placed in the hole, sealed with uncured kwik sil (WPI), and fixed to the skull using Super-bond (DSM Dentaire).

Imaging procedure

Mice were head-fixed on a non-motorized treadmill (adapted from (Royer *et al.*, 2012)) allowing them self-paced locomotion to limit stress, and all experiments were performed in the dark. No rewards were given and the mice alternated between periods of moving and resting activity during recordings. Contralateral electrodes were connected to a multi-channel amplification system (xCellAmp_32c, Dipsi) and these signals along with the temporal PMT trigger and treadmill speed signal were digitalized at 2 kHz through a 1440A Digidata (Axon instrument), amplified 2500 times, and visualized using Axoscope 10 (Axon instrument). Imaging was performed with a single beam multi-photon pulsed laser scanning system coupled to a microscope (TriM Scope II, LaVision Biotech). The Ti:sapphire excitation laser (Chameleon Ultra II, Coherent) was operated at

920 nm (< 20 mW average power in the sample). GCaMP fluorescence was isolated using a bandpass filter (510/25). Images were acquired through a GaSP PMT (H7422-40, Hamamatsu) using a 16x immersion objective (NIKON, NA 0.8, *n* = 9 mice) or 20x immersion objective (Olympus, NA 1.0, *n* = 1 mouse). Using Imspector software (LaVision Biotech), the fluorescence activity from a 400x400 μm field of view (500x500 μm for 20x objective) was acquired at ~7.7 Hz range (7.5-9.7 Hz) and recordings lasted ~4.5 min. Imaging fields were selected to sample the dorsal CA1 area at depths from 10-150 μm relative to the fiber surface (range spans *stratum oriens* and *stratum pyramidale*). Multiple movies spanning the CA1 region were taken during each recording session and mice were imaged over multiple days (range 2-16 days). During imaging sessions, mice displayed spontaneous interictal spikes as detected in the cEEG signal and these spike times were aligned with the corresponding movie frames through post hoc analysis as described above.

Movement correction and noise subtraction

After acquisition, all fluorescence movies were aligned to correct for movement in the x-y plane using a two-iteration cross-correlation based registration in Matlab. For a given iteration, movement correction was limited to 10 pixels in either direction, except for rare cases of extreme movement when the tolerance was increased to 20 pixels for the first iteration. The 20 pixels on each edge of the movie were cropped from each frame of the movie so that edge effects would not be present in the further analysis. Additionally, the background noise present in the PMT was estimated and subtracted from all frames in order to reduce noise artifacts when calculating dF/F images.

Single-cell activation during ripple events

For experiments involving the imaging of ripple events, wild type, non-epileptic Swiss mice (*n* = 2) were implanted with a chronic hippocampal window, following the same procedure as for TLE mice. Again as in TLE mice, non-epileptic mice were implanted with a cLFP placed in the CA1 *stratum pyramidale* , however, no cortical surface EEG electrode was implanted. Imaging was performed under the same

conditions as TLE mice, and ripples were detected from spectrograms of cLFP activity, created using wavelet decomposition with a Morlet wavelet with a scaling factor of ¼.

Spatial imprints

For the calculation of the spatial imprint of calcium activation associated with each interictal spike, the movie frames corresponding to a 500 ms window immediately preceding (but not including) the spike were selected to represent the baseline activity before each event. Similarly, the frames corresponding to a 500 ms window immediately after (and including) the spike were selected to represent the activity associated with the interictal spike. For each window (before and after) the sequence of images was averaged to produce a single image of activity both before and after the spike (denoted as F_b and F_a respectively). We then calculated the spatial imprint of each event by calculating the dF/F image for the event, ie, for each pixel, we calculated the change in fluorescence as (F_a-F_b)/F_b. This results in a normalized single image where pixels that were active (experienced an increase in fluorescence) during the event appear brighter than those that were not active.

Single cell activity analysis in calcium imaging movies

For each mouse, we selected the two movies in the *stratum oriens* and two movies in the *stratum pyramidale* that had the highest number of detected interictal spikes for further analysis of activity at the level of individual cells. The strategy for detecting cell contours varied between the two regions due to the intrinsically different properties of cell size and location in the *stratum oriens* versus *stratum pyramidale*. Importantly, due to the high packing of cells in the *stratum pyramidale* (Fig 3D), we were only able to detect cells that displayed an increase in the GCaMP signal (ie, were active) at some point in time during the movie. Thus, the detected cells in the *stratum pyramidale* reflect only the active cells, while in the *stratum oriens*, they represent all cells present in the imaging field. However, we estimated the total number of pyramidal cells in the imaging field by calculating the total area of the *stratum pyramidale* and dividing by the average area of a single cell (calculated by averaging the area enclosed detected active cells' contours; see next section). For the purpose of visualization of events in Fig. 3E,

contours of cells in the *stratum pyramidale* were manually identified for a single movie and examples of cellular recruitment were shown for 4 interictal spikes from this movie.

For each movie, we first computed a series of 7 images reflecting various properties of the time series of calcium fluorescence of each pixel. We examined the average image (each pixel represented by its average value), maximum image (each pixel represented by its maximum value), maximum dF/F image (each pixel represented by its maximum dF/F value), correlation image (each pixel represented by its average Pearson correlation with its nearest neighbors), covariance image (each pixel represented by its average covariance with its nearest neighbors), normalized correlation image (each pixel represented by its average normalized correlation with its nearest neighbors) and skewness image (each pixel represented by the skewness of its signal). For detection of active cells in the *stratum pyramidale*, the maximum dF/F image and skewness images were visually inspected for manual labeling of cell contours. In the *stratum oriens*, we were able to detect all cells in the imaging field through visual inspection and comparison of all 7 images, and cell contours were manually labeled.

To determine whether or not a cell was active during an interictal spike, we first calculated the average image dF/F of each spike by calculating the maximum value of the average fluorescence signal (averaging done over the visible portion of the imaging field that contained either the *stratum pyramidale* or *stratum oriens*) in a 500 ms window after the spike and using the average value of the same signal during a 500 ms window preceeding the spike as a baseline. In order to analyze interictal spikes with a visible response in the calcium imaging, we additionally selected only spikes in which this value was greater than 50% (referred to as "large interictal spikes"). If the dF/F for an individual cell was greater than the dF/F averaged over the image during the spike, the cell was determined to participate in the interictal spike.

Estimated percentage of active pyramidal cells

Due to the dense packing of cells in the *stratum pyramidale* and the fact that GCaMP is excluded from the nucleus of pyramidal cells, images from calcium movies recorded in the *stratum pyramidale* resembled densely packed, overlapping donuts, making it difficult to determine individual cell contours. For single-cell analysis, we

therefore only detected cells that were active during a given movie, as their transient increase in GCaMP fluorescence made the detection of the cellular contour possible. We estimated the total number of pyramidal cells in the imaging field by calculating the total area of the *stratum pyramidale* and dividing by the average area of a single cell (calculated by averaging the area enclosed detected active cells' contours). We then calculated the average estimated percentage of active cells for movies imaged from mice injected with GCaMP5G to be 1.8 ± 0.8% (n = 6 movies from 3 mice) and 7.5 ± 1.2% for mice injected with GCaMP6 (n = 6 movies from 3 mice). Due to these low percentages of total active cells, for the *stratum pyramidale*, we additionally reported percentages of cells active during interictal spikes calculated from the number of detected cells, not total estimated cells. These results are summarized in Table 1 of the main manuscript where we additionally list the number and percentage of cells active outside of the interictal spikes. We did not attempt to do this calculation for interneurons located in the *stratum oriens* because it was often the case that an interneuron was only observed to be active during the interictal spike. Therefore, the number of cells active during the interictal spike could be greater than the number active outside of the event.

Curve fitting and comparison of wild type vs GAD67-Cre groups

To determine the relationship between the cEEG amplitude (denoted x below) and average Ca response (denoted y below) during interictal spikes, for each animal (n = 3 GCaMP5, n = 3 GCaMP6, n = 4 GAD67-Cre), curves were fit to the following equation in Malab: $y = ax^2 + bx + c$. We chose this supralinear equation because we know that the expected fluorescence response of the GCaMP indicator as a function of the number of action potentials fired by a neuron is supralinear based on previous calibrations (Akerboom *et al.*, 2012). Assuming that the amplitude of the cEEG spike reflects the firing rate of the neurons, we would thus expect curve for the observed fluorescence response as a function of the cEEG amplitude to also be supralinear. Optimal parameters were determined using the following constraints: 1) $y(0) = 0$ and 2) $y > 0$ for all x in order to conform to experimental expectations of the GCaMP response. We also note that the supralinear fit was superior to a linear fit when assessed using the adjusted R^2

values (adjusted R^2 = 0.30 ± 0.03 for a linear fit; adjusted R^2 = 0.46 ± 0.02 for a supralinear fit).

Differences between the response curves for wild type and GAD67-Cre mice were assessed using Functional Data Analysis (Ramsay and Silvermann, 2005) Specifically, a non-parametric permutation test (Bassett *et al.*, 2012) was employed by calculating the average curve for each group (wild type, n = 6 or GAD67-Cre, n = 4) and then computing the area between the two average curves for cEEG values ranging from 0 – 2 mV. Surrogate data sets were then created by randomly re-assigning each curve to be in either the wildtype or GAD67-Cre group and repeating the above calculation. This yielded a distribution of values for the area between curves that was then used to compute significance by counting the number of data points in the surrogate set that were above the value calculated from the data and dividing by the total number of surrogates. Here, 10,000 surrogate sets were used.

Spatial similarity of events

In order to determine similarity between the spatial patterning of activation during interictal spikes, we developed a four stage process:

1. The average image dF/F signal for each spike was calculated as described above for determining cellular activity, and this value was used as a threshold to create binary representations of the spatial imprint in which pixels above the threshold were set to 1 and pixels below the threshold were set to 0 (Fig. 4a-b). The binarization was performed in order to isolate the spatial structure of events and eliminate any amplitude dependent effects in further calculations of similarity.
2. A pairwise matrix of similarity was then calculated using the minimum of the two Manders colocalization coefficients, M_1 and M_2 (Manders *et al.*, 1993). The Manders colocalization coefficients are commonly used to assess colocalization and calculate the percentage of overlap between two images.
3. Similarity matrices were sorted using average linkage hierarchical clustering (Fig. 5c) and the similarity matrices were visualized to reflect the sorting order (Fig. 5d).

4. Communities of events with similar structure were visually detected as block-like groupings along the diagonal of the sorted similarity matrix (Fig. 5d).

This analysis was carried out only for movies in the *stratum oriens* of GAD67-Cre mice because of the increased signal-to-noise ratio due to the lack of background. It should also be noted that this type of analysis could only be performed on events contained within a single movie (and therefore from the same imaging plane). Additionally, analysis was only performed on large interictal spikes (defined previously) and carried out in movies that contained 5 or more large interictal spikes.

Correlations between correlated cEEG and overlap of spatial patterning

To assess correlations between the shape of the cEEG signal during interictal spikes, a 500 ms window centered on each spike was extracted, and the maximum value of the pairwise normalized cross-correlation performed over a maximum lag value of 250 ms was calculated. This created a pairwise matrix representing the similarity of the spatial structure of the cEEG between interictal spikes, similar to the similarity matrix created for the spatial imprints described above. The correlation between the cEEG similarity matrix and the spatial similarity matrix was assessed using a standard Pearson's correlation.

Assessing the sensitivity of GCaMP5/6 signals to action potential firing in *stratum pyramidale* CA1 neurons

Mice (n = 28) were injected as previously described, and 12-17 days after virus injection, surgery was performed on mice deeply anesthetized with ketamine (100 mg /kg) and xylazine (10 mg /kg). An analgesic (Buprenorphine, 0.1mg/kg) was administrated sub-cutaneously. Body temperature was kept constant by a heating pad and breathing rate visually monitored. A reference electrode was placed above the contralateral cerebellum. An asymetric craniotomy was performed above and posterior to the injection sites in order to insure enough space for pipette insertion. The overlying cortex was withdrawn and a buffered saline (D-PBS, Sigma) was used to irrigate the tissue. A custom designed glass coverslip containing a laser-cut hole that allowed for pipette insertion was placed above the hippocampus.

After surgery, mice were transferred to the recording setup where body temperature was continuously monitored. A supplemental anesthetic was provided when necessary (urethane, 1.5g/kg, Sigma). A solution of aCSF [containing (in mM): 126 NaCl,3.5 KCl, 1.2 NaH2PO4, 26 NaHCO3, 1.3 MgCl2, 2.0 CaCl2, and 10 D-glucose, pH 7.4] and Alexa Fluor 594 (Life Technologies) was freshly prepared and loaded in borosilicate glass pipettes (4-15mΩ, tip diameter 1-2µm). A second PMT (Hamamatsu, H6820) was used to locate the pipette tip. The glass pipette slowly entered the tissue through the hole using a 31 ± 1° approach angle at a maximal speed of 10µm/sec under constant visual and electrophysiological inspection. Upon reaching the pyramidal cell layer, the speed was decreased and spontaneous cell activity in both imaging and electrophysiological recordings was monitored. Stable juxtacellular recordings were acquired with a MultiClamp 700B Amplifier (Axon Instrument) and digitized at 20kHz (Digidata1440a, Axon Instrument). Imaging was performed with a 16x objective (NIKON, NA 0.8) at 7-14Hz (100-250 µm, 102-254 pixel).

Our success rate was limited by mortality during experiments, low quality optical and electrophysiological signals, lack of spontaneous activity, as well as high bleeding. The strongest limiting factor was the difficulty to identify the juxtacellularly recorded neurons due to the high cell density. We achieved reliable recordings in 4 neurons recorded from 3 different mice (GCaMP5: n = 1 neuron and GCaMP6: n = 3 neurons).
Analysis was performed using custom-made software (Matlab, MathWorks). In brief, spikes were detected using a threshold value of 5 times the standard deviation of the bandpass filtered signal (100-6000 Hz). A spike waveform analysis was applied to verify that all action potentials were issued by the same neuron. Spikes separated by less than 15 ms were considered to occur within the same burst. Bursts separated by less than 2 frames were discarded. DF/F was calculated as the difference between the peak fluorescence amplitude within 3 frames following the burst onset and the baseline, normalized to the baseline. (The baseline was calculated by averaging the fluorescence signal over a 250 ms period immediately before the burst onset.) Results are displayed as mean ± s.e.m.

Comment on imaging spontaneous seizures in TLE mice

Although TLE mice display spontaneous seizures during the chronic phase of the pilocarpine model, the frequency of seizures is relatively low (as observed in our previous work using telemetric EEG to monitor seizure activity (Feldt Muldoon *et al.*, 2013)), and therefore the probability of a seizure occurring during an imaging session is quite low. In fact, despite the many hours of imaging presented in this study, even when including periods of time with only electrophysiological recordings, we only recorded two seizures in the electrophysiology. One of these seizures occurred during an imaging session in the *stratum pyramidale* of a preliminary animal with poor optical resolution so no results from this animal were reported in the main manuscript. We include data from this preliminary animal here, but would like to emphasize that few conclusions should be drawn from this single example. This seizure also occurred in a WT mouse so we had no ability to separate the GABAergic signal from the glutamatergic signal. However, we did observe what appeared to be a diffusive wave of fluorescence that spread across the imaging area midway through the tonic phase and flashed in sync during the tonic phase of the seizure (Supplementary Fig. 7). The second seizure started during final few seconds of an imaging session and we were unable to restart the imaging to capture the activity, but the electrophysiology for this seizure is displayed in Fig. 1A of the main manuscript. The imaging of neuronal participation in spontaneous seizure activity would be incredibly interesting and insightful, and future work should further attempt this difficult endeavor.

Supplementary Figure Captions

Supplementary Figure 1: Description of methods. (A) Timeline of the pilocarpine mouse model of TLE. All recordings were done during the chronic phase of the model where mice exhibited spontaneous seizures and interictal spikes. (B) Depiction of method for detecting interictal spikes. Potential spikes were first identified as points where the filtered signals of the cEEG and cLFP were outside of the moving window threshold (dashed boxes). These points were then compared to the EMG signal to separate true spikes from movement artifacts (black star denotes true spike) and the start and end times for each spike were marked (red stars). (C) Schematic depicting the area

of cortex removed and implantation of the chronic imaging window. (D) Head-restrained mouse in imaging set-up. The mouse is free to run on a linear treadmill. (E) Creation of spatial imprints. The movie frames in a 500 ms window immediately before the interictal spike are averaged to create a "before image" and the movie frames in the 500 ms window including and immediately after the spike are averaged to create an "after image". The spatial imprint is calculated by a pixel-by-pixel subtraction of the before image from the after image, normalized by the before image. Thus, pixels activated during the interictal spike appear as bright in the spatial imprint. The red arrow indicates a cell that is not activated in the spike, while the green arrow indicates a cell that is activated during the spike.

Supplementary Figure 2: Histological characterization of GCaMP5G expressing cells. **(**A) Photomicrographs comparing the GCaMP5G signal (green, left) and the immunostaining for NeuN to label the somata of all neurons (magenta, middle) in the CA1 area. Image superimposition is displayed on the right panel with inset showing the *stratum pyramidale* at a higher magnification. Note that all the magenta nuclei are surrounded by green GCaMP5 signal in the cytoplasm. (B) GFAP staining for astrocytes does not colocalize with the GCaM5G signal. (C) Photomicrographs of the GCaMP5G signal from the CA1 *stratum pyramidale* imaged *in vivo* in a GAD67-Cre /Ai14 mouse (Cre- dependent TdTomato reporter). GABAergic neurons are represented in magenta. (D) GABAergic neurons from a GAD67-Cre mouse injected with the floxed version of the GCaMP5G viral vector (green). Neurons are indicated with NeuN immunostaining (magenta). (E) Histogram representing the fraction of GCaMP5G expressing cells among neurons (7578 neurons, n = 2 mice) and astrocytes (784 GFAP+ cells, n = 2 mice). (F) Histogram representing the fraction of GAD67 positive neurons in the dorsal CA1 pyramidal cell layer from *in vivo* (left, 4822 neurons, n = 5 mice) and *ex vivo* staining (right, 4329 neurons, n = 3 mice). (G) Histogram plotting the absolute number of neurons and GAD67 positive neurons in a 400 x 400 µm field of view counted using *in vivo* images in the *stratum pyramidale* of a control GAD67-Cre mouse. Results are expressed as mean ± s.e.m. Scale bar: 100µm.

Supplementary Figure 3: Linear probe schematic and diI track showing probe placement. Scale bar: 100µm.

Supplementary Figure 4: Calcium imaging of CA1 multineuron activity. (A) Image of the GCaMP5G signal in the *stratum pyramidale*; Scale bar: 100µm. Contours (black) indicate detected active cells. (B) GCaMP5G signal of cells from (A) and corresponding cEEG, EMG and speed recordings (Supplementary Video 1). Scale: cEEG = 2mV, EMG = 4mV, Speed = 20 cm/s.

Supplementary Figure 5: Calcium activity of three neurons correlated to a ripple event. Top: Fluorescence trace of three neurons in a 2.5 s window around a ripple event (dots indicate the timing of imaging frames). Inset: Fluorescence trace of the same neurons in a 20 s window around a run episode (note the different dF/F scale indicating a greater calcium response during activation outside of the event). Middle: Wavelet spectrogram of the cLFP (raw data in white) for the same 2.5s window. The black dotted line represents the ripple onset time. Bottom: Same graph as above for a 200 ms window highlighting the ripple event.

Supplementary Figure 6: GCaMP5/6 signals in *stratum pyramidale* CA1 neurons and their relationship to action potentials. (A) Median (thick line) and interquartile range (red area) of the fluorescence signal as a function of the number of action potentials (from 1 to 5) per burst in a neuron expressing GCaMP5G. The start of the burst as recorded electrophysiologically is used for a reference. Baseline noise is indicated by the green dashed line. (B) Intensity map of the field of view indicating the position of the recording pipette (white) and of the imaged neuron (red); scale bar: 50µm. (C) Median (thick) and 10^{th}-90^{th} percentile (red area) of the spike waveform. (D) Fluorescence change as a function of the number of action potentials per burst. Mean ± s.e.m. is indicated; single events are indicated by open dots. Numbers of recorded bursts are given in brackets. Noise level is indicated by the green dashed line. (E-H) Same as (A-D) for a neuron expressing GCaMP6M.

Supplementary Figure 7: Calcium imaging in the *stratum pyramidale* of a spontaneous seizure in a preliminary mouse. Top: Heat map representation of the dF/F signal in individual cells. Middle: Fluorescence signal summed over entire imaging area during the seizure. Bottom: cEEG signal of observed seizure. Note that in this mouse, it was impossible to separate the glutamatergic and GABAergic contributions to the observed fluorescence response.

Supplementary Video Captions

Supplementary Video 1: Imaging in the *stratum pyramidale* during normal activity. Movie of fluorescence signal from the *stratum pyramidale* of a mouse injected with GCaMP5 showing pyramidal cell activity, cEEG, EMG, and speed of mouse on treadmill during a period free of interictal spiking. Cells are active (seen as a transient increase in fluorescence) both when the mouse is moving and while at rest, although more activity is apparent during periods of motion.

Supplementary Video 2: Imaging in the *stratum pyramidale* during an interictal spike. Movie of fluorescence signal from the *stratum pyramidale* of a mouse injected with GCaMP5 alongside simultaneously recorded cEEG, EMG, and average image fluorescence signal during an interictal spike (denoted by dashed red line). One cell appears active during the spike along with the transient overall flash, and other cells show activity as the mouse begins to move after the spike.

Supplementary Video 3: Imaging in the *stratum oriens* during an interictal spike. Movie of fluorescence signal from the *stratum oriens* of a mouse injected with GCaMP5 alongside simultaneously recorded cEEG, EMG, and average image fluorescence signal during an interictal spike (denoted by dashed red line). A web of neuronal processes and multiple cell bodies are recruited during the spike.

Supplementary Video 4: Imaging of GABAergic neurons in the *stratum pyramidale* during an interictal spike. Movie of fluorescence signal from the *stratum pyramidale* of a GAD67-Cre mouse where only GABAergic cells express GCaMP5 alongside simultaneously recorded cEEG, EMG, and average image fluorescence signal during an interictal spike (denoted by dashed red line). Importantly, all observed increases in the fluorescence signal come from only GABAergic cells. The interictal spike is seen as a transient overall flash through the perisomatic innervation in the *stratum pyramidale*.

Supplementary Video 5: Imaging of GABAergic neurons in the *stratum oriens* during an interictal spike. Movie of fluorescence signal from the *stratum oriens* of a GAD67-Cre mouse where only GABAergic cells express GCaMP5 alongside simultaneously recorded cEEG, EMG, and average image fluorescence signal during an interictal spike (denoted by dashed red line). As in Supplementary Video 3, a web of GABAergic processes and cell bodies are recruited during the spike.

Reference List

Akerboom J, Chen TW, Wardill TJ *et al*. Optimization of a GCaMP calcium indicator for neural activity imaging. J Neurosci 2012; 32: 13819-13840.

Bassett DS, Nelson BG, Mueller BA, Camchong J, Lim KO. Altered resting state complexity in schizophrenia. Neuroimage 2012; 59: 2196-2207.

Dombeck DA, Harvey CD, Tian L, Looger LL, Tank DW. Functional imaging of hippocampal place cells at cellular resolution during virtual navigation. Nat Neurosci 2010; 13: 1433-1440.

Feldt Muldoon S., Soltesz I, Cossart R. Spatially clustered neuronal assemblies comprise the microstructure of synchrony in chronically epileptic networks. Proc Natl Acad Sci U S A 2013; 110: 3567-3572.

Manders EMM, Verbeek FJ, Aten JA. Measurement of Colocalization of Objects in Dual-Color Confocal Images. Journal of Microscopy-Oxford 1993; 169: 375-382.

Potworowski J, Jakuczun W, Leski S, Wojcik D. Kernel Current Source Density Method. Neural Computation 2012; 24: 541-575.

Ramsay J, Silvermann BW. Functional Data Anlaysis. Springer; 2005.

Royer S, Zemelman BV, Losonczy A *et al*. Control of timing, rate and bursts of hippocampal place cells by dendritic and somatic inhibition. Nat Neurosci 2012; 15: 769-775.

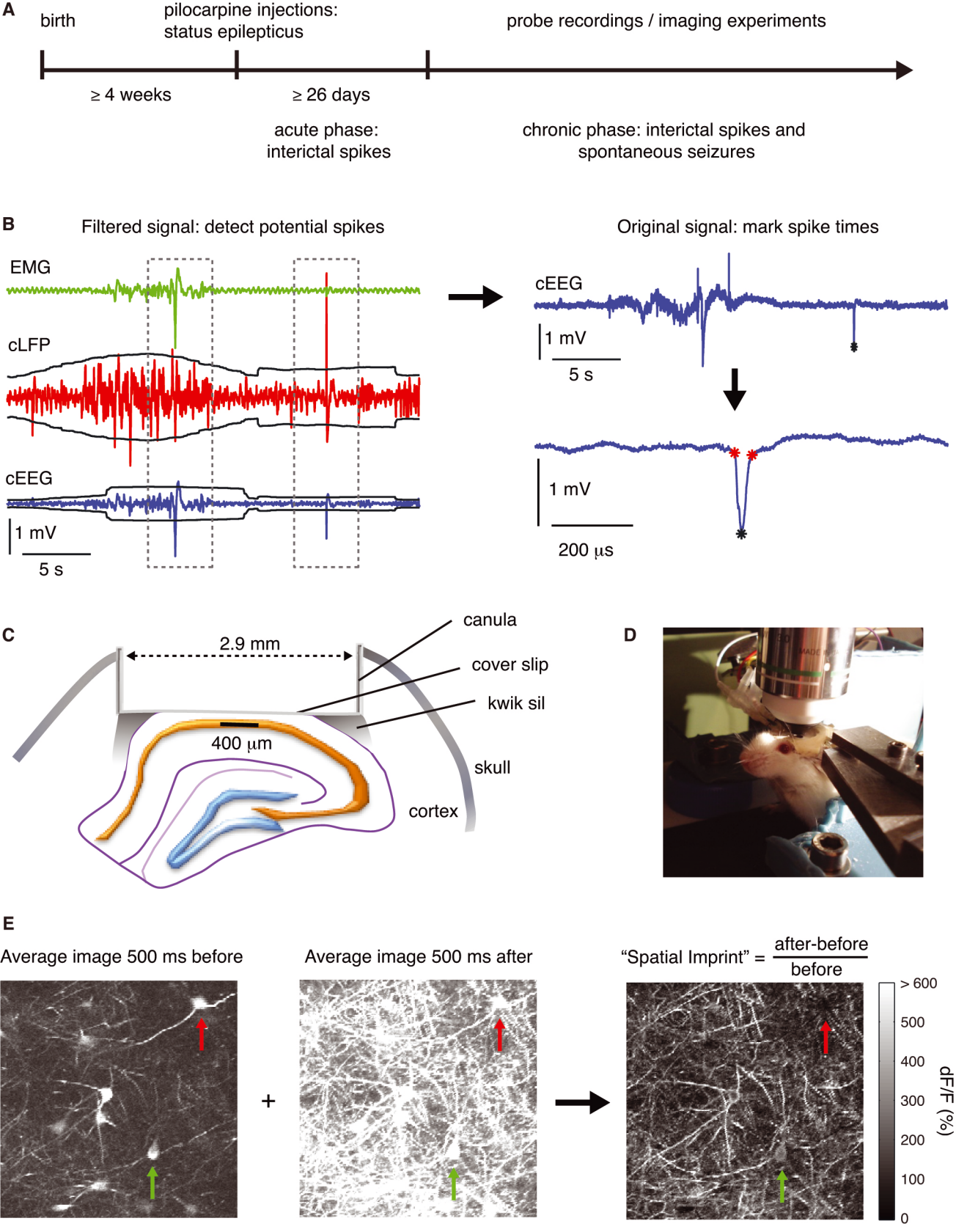
A
birth
pilocarpine injections:
status epilepticus
probe recordings / imaging experiments
≥ 4 weeks
≥ 26 days
acute phase:
interictal spikes
chronic phase: interictal spikes and
spontaneous seizures
B
Filtered signal: detect potential spikes
Original signal: mark spike times
EMG
cLFP
cEEG
1 mV
5 s
cEEG
1 mV
5 s
1 mV
200 µs
C
2.9 mm
canula
cover slip
kwik sil
400 µm
skull
cortex
D
E
Average image 500 ms before
Average image 500 ms after
"Spatial Imprint" = after-before / before
> 600
500
400
300
200
100
0
dF/F (%)

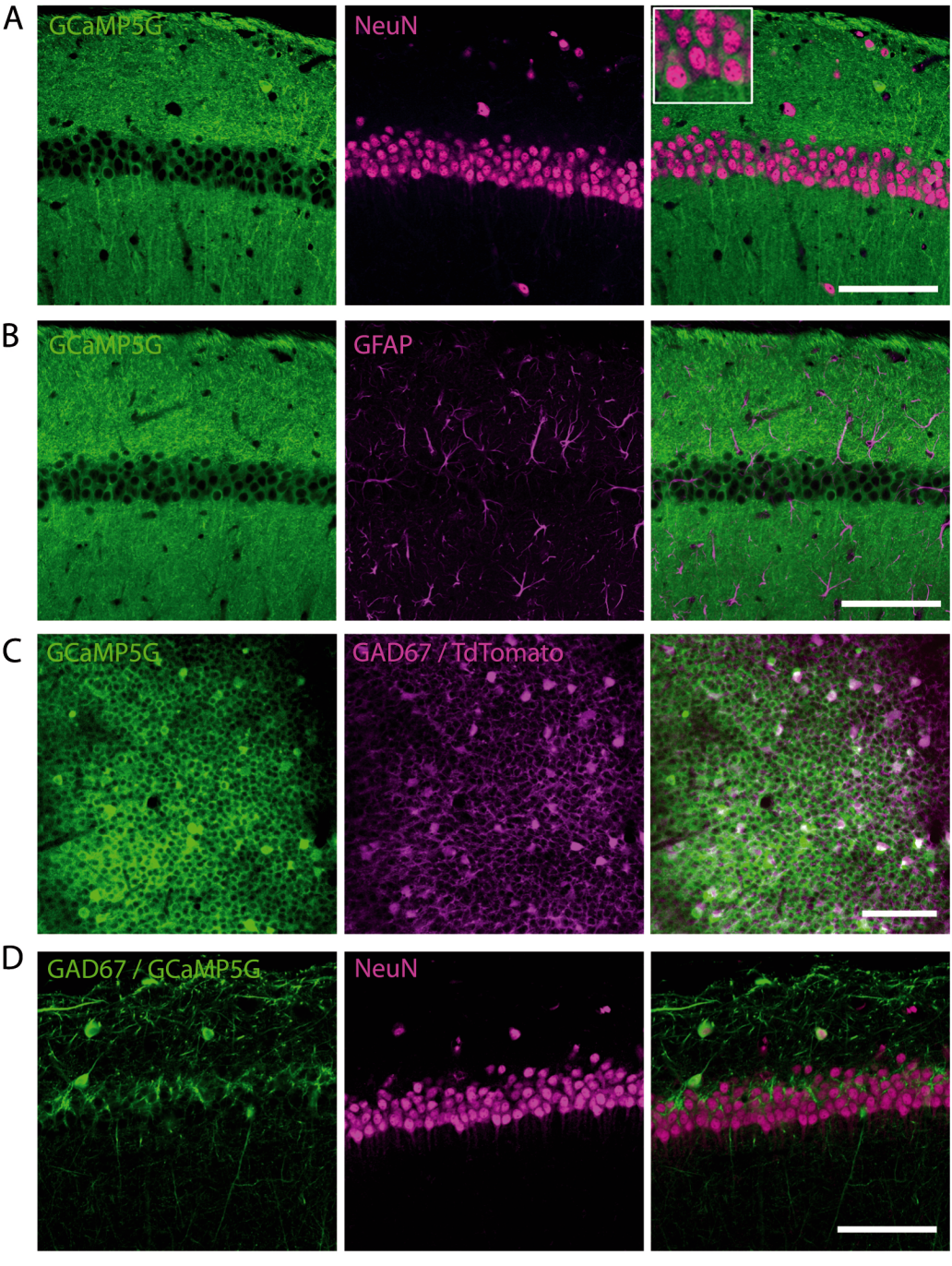
A
GCaMP5G
NeuN
B
GCaMP5G
GFAP
C
GCaMP5G
GAD67 / TdTomato
D
GAD67 / GCaMP5G
NeuN

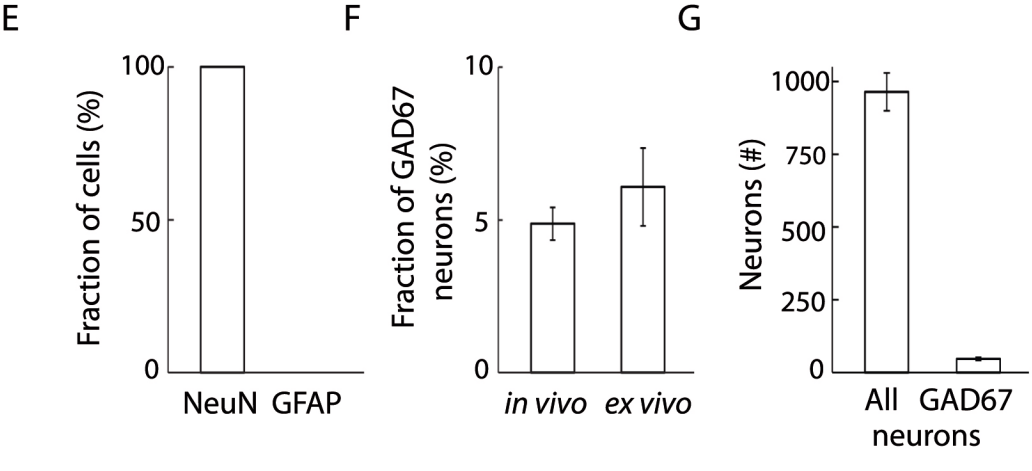
E
Fraction of cells (%)
100
50
0
NeuN
GFAP
F
Fraction of GAD67 neurons (%)
10
5
0
in vivo
ex vivo
G
Neurons (#)
1000
750
500
250
0
All neurons
GAD67

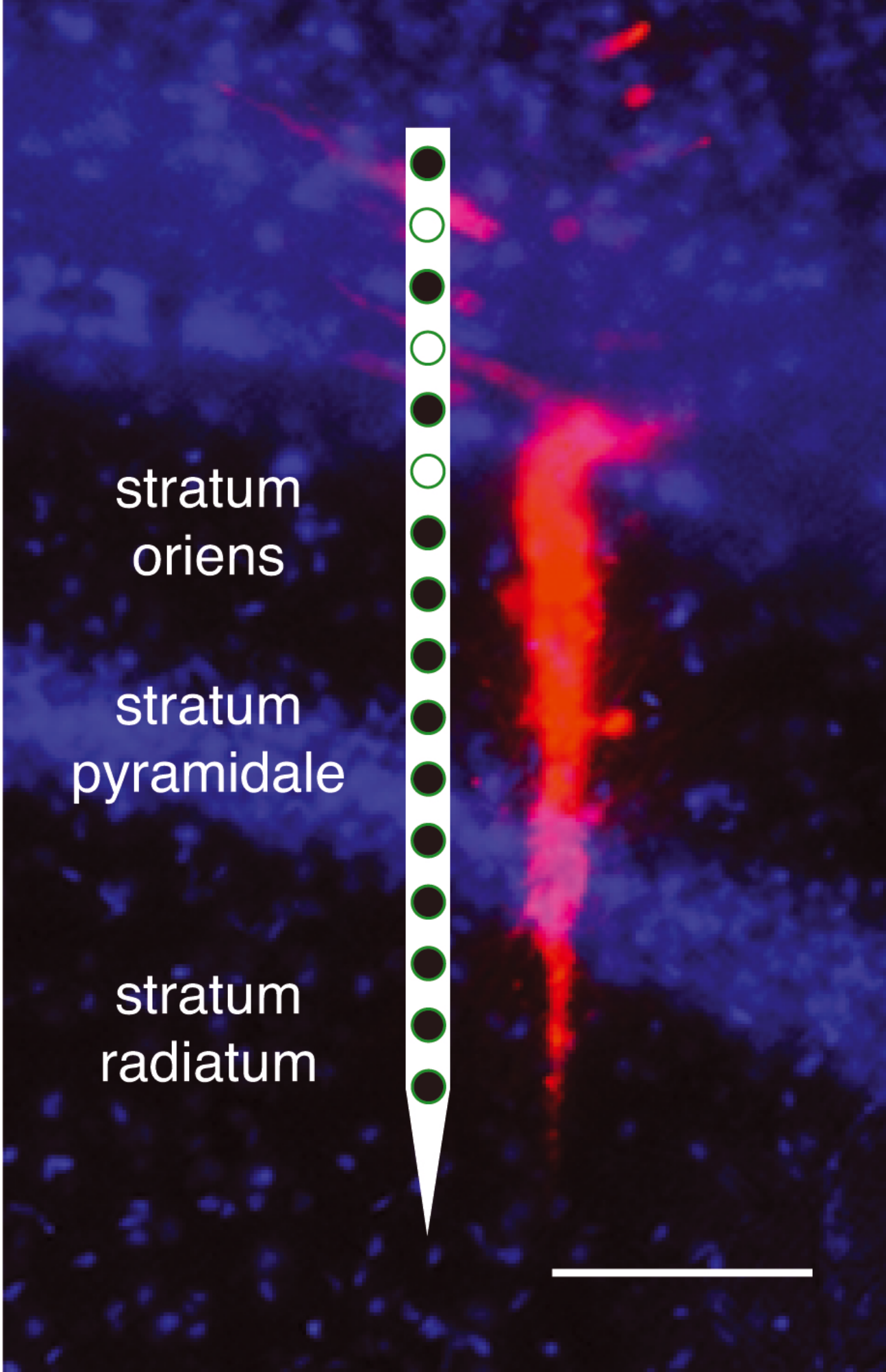
stratum
oriens
stratum
pyramidale
stratum
radiatum

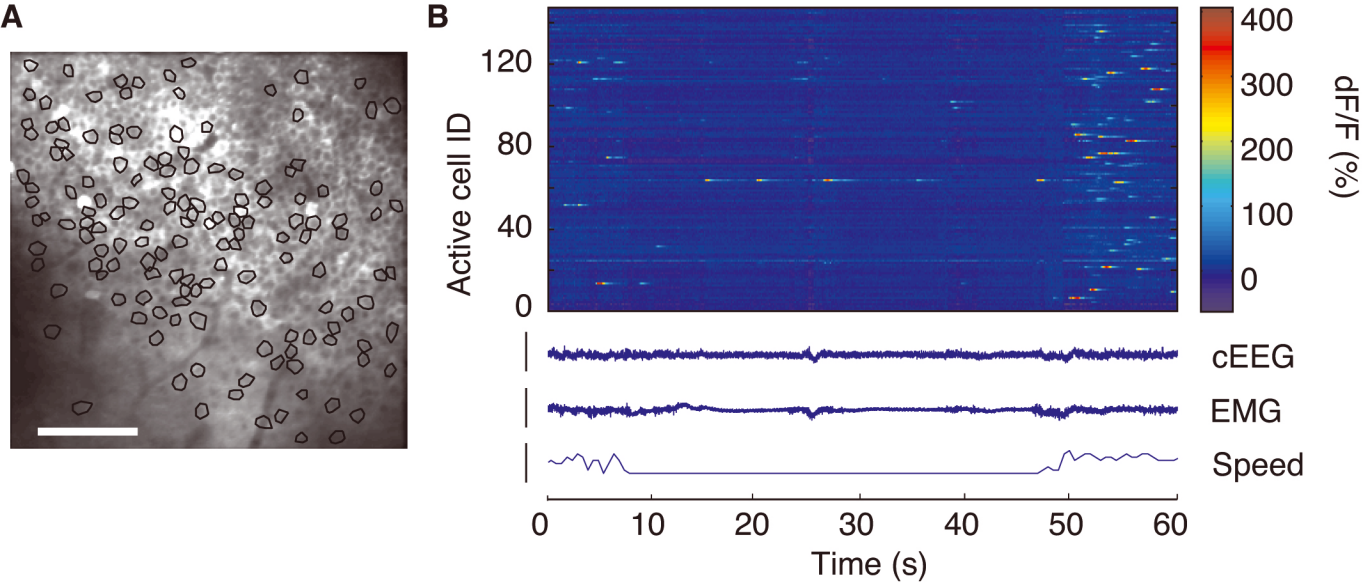
A
B
Active cell ID
120
80
40
0
400
300
200
100
0
dF/F (%)
cEEG
EMG
Speed
0
10
20
30
40
50
60
Time (s)

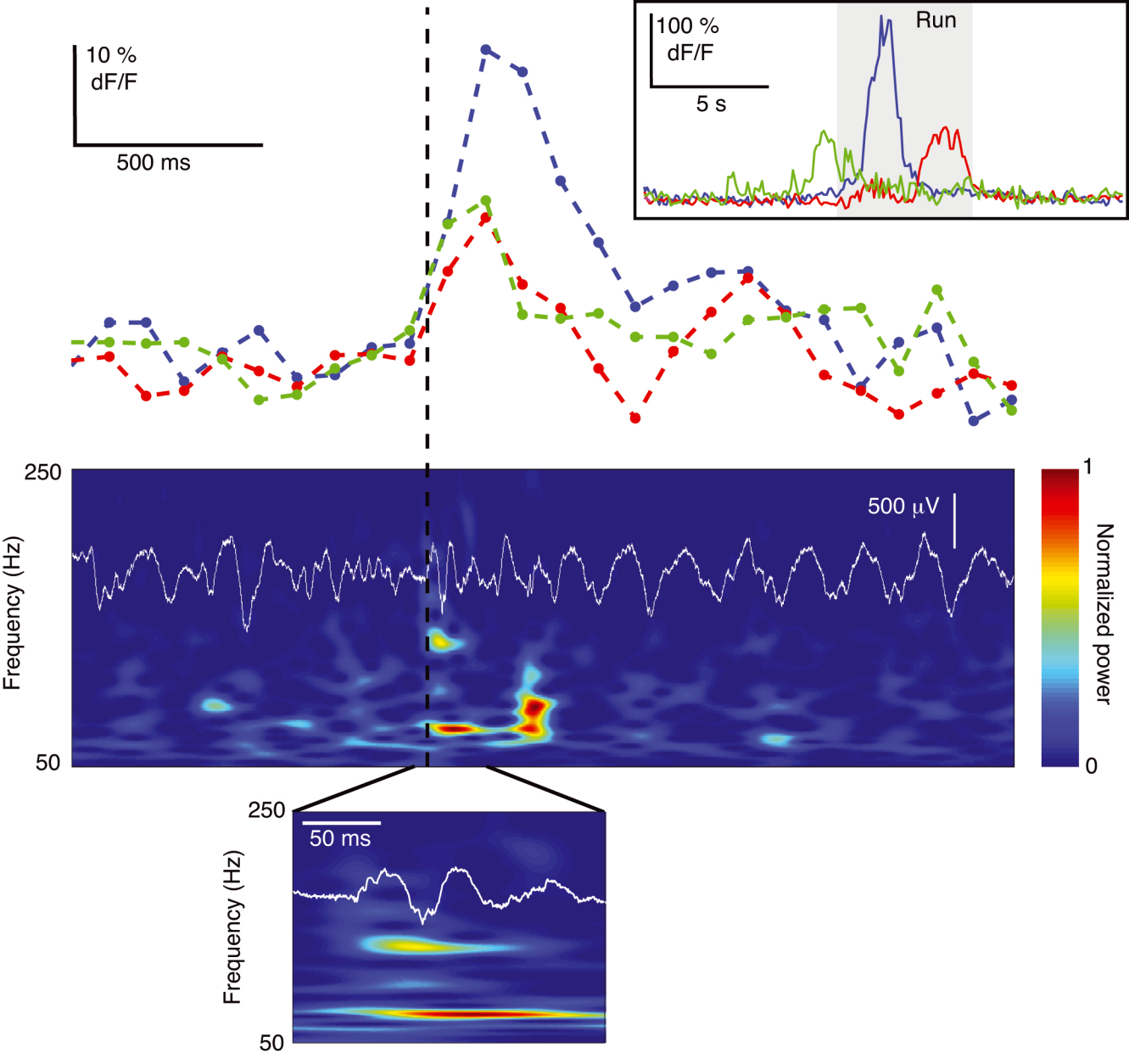
10 %
dF/F
500 ms
100 %
dF/F
5 s
Run
250
Frequency (Hz)
50
500 μV
1
Normalized power
0
250
50 ms
Frequency (Hz)
50

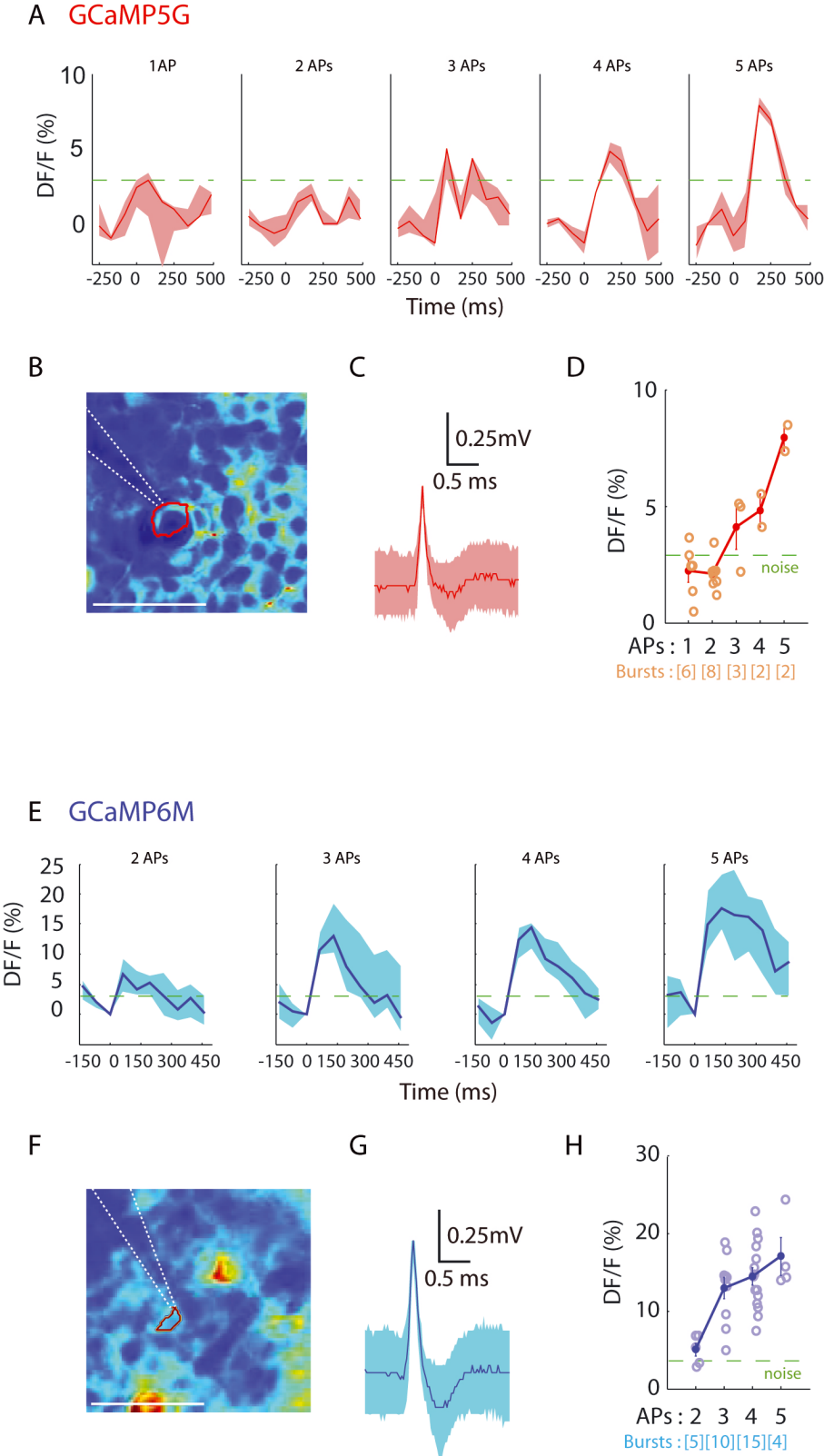
A
GCaMP5G
1AP
2 APs
3 APs
4 APs
5 APs
DF/F (%)
10
5
0
-250 0 250 500
Time (ms)
B
C
0.25mV
0.5 ms
D
DF/F (%)
noise
APs : 1 2 3 4 5
Bursts : [6] [8] [3] [2] [2]
E
GCaMP6M
2 APs
3 APs
4 APs
5 APs
DF/F (%)
25
20
15
10
5
0
-150 0 150 300 450
Time (ms)
F
G
0.25mV
0.5 ms
H
DF/F (%)
30
20
10
0
noise
APs : 2 3 4 5
Bursts : [5][10][15][4]

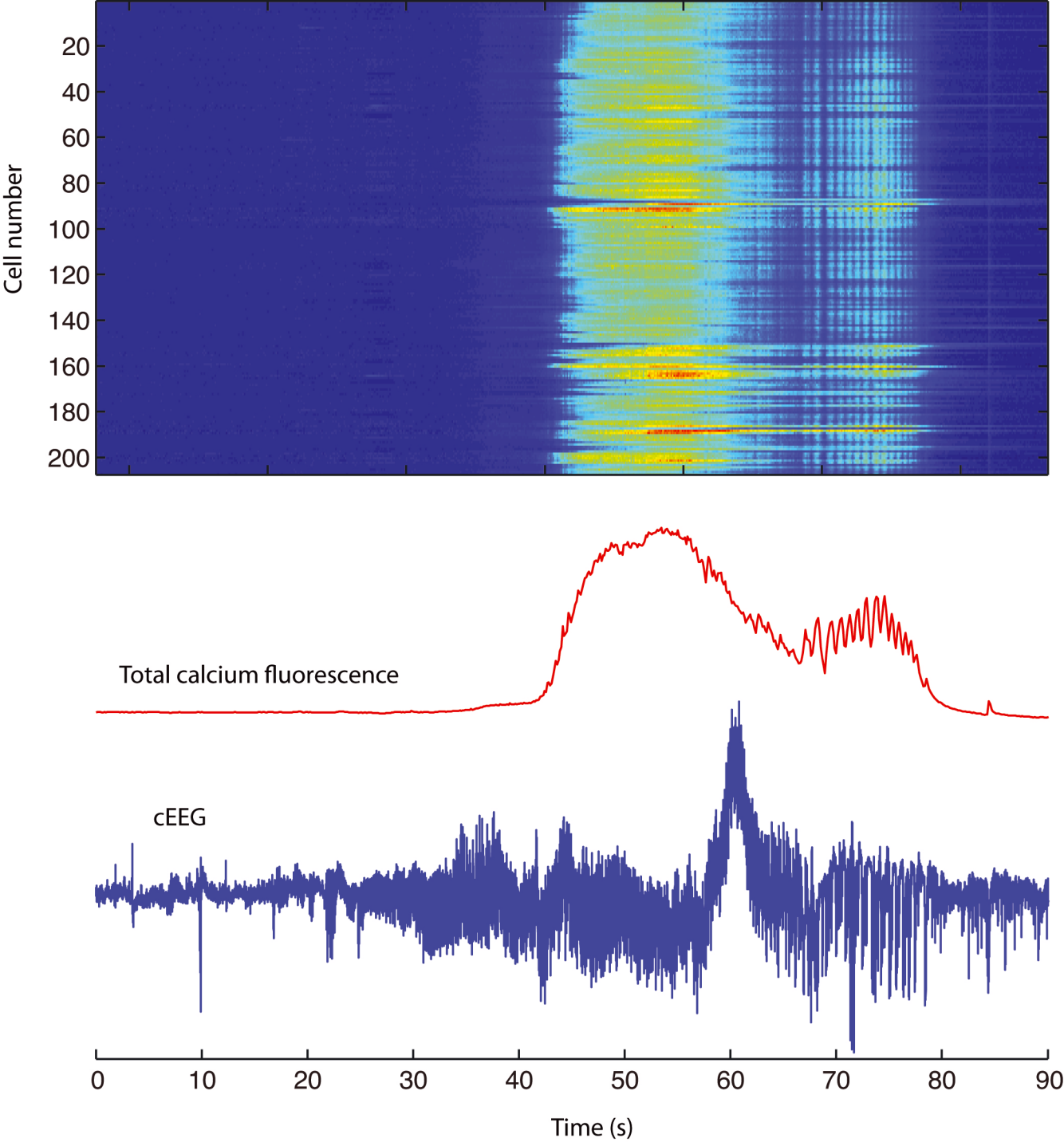
Cell number
20
40
60
80
100
120
140
160
180
200
Total calcium fluorescence
cEEG
0
10
20
30
40
50
60
70
80
90
Time (s)